THE JOURNAL OF BIOLOGICAL CHEMISTRY VOL. 289, NO. 32, pp. 21828–21843, August 8, 2014

Bidirectional Modulation of Thermal and Chemical Sensitivity of TRPM8 Channels by the Initial Region of the N-terminal Domain*[S]

Received for publication, March 17, 2014, and in revised form, May 5, 2014 Published, JBC Papers in Press, June 10, 2014, DOI 10.1074/jbc.M114.565994

María Pertusa[‡§1], **Alejandro González**[‡], **Paulina Hardy**[‡], **Rodolfo Madrid**[‡], **and Félix Viana**[§]

From the [‡]*Departamento de Biología, Facultad de Química y Biología, Universidad de Santiago de Chile, 9160000 Santiago, Chile and the* [§]*Instituto de Neurociencias de Alicante, Universidad Miguel Hernández-Consejo Superior de Investigaciones Científicas, 03550 Alicante, Spain*

Background: The functional role of the TRPM8 N terminus remains poorly understood.
Results: Truncation of the first 40 residues increases TRPM8 responses to cold and menthol, whereas deletions within the 40–60-residue region yield nonfunctional channels retained in the ER.
Conclusion: Initial N terminus of TRPM8 is important for proper biogenesis and function.
Significance: Variations within the N terminus can modulate thermal and chemical sensitivity of TRPM8.

TRPM8, a nonselective cation channel activated by cold, voltage, and cooling compounds such as menthol, is the principal molecular detector of cold temperatures in primary sensory neurons of the somatosensory system. The N-terminal domain of TRPM8 consists of 693 amino acids, but little is known about its contribution to channel function. Here, we identified two distinct regions within the initial N terminus of TRPM8 that contribute differentially to channel activity and proper folding and assembly. Deletion or substitution of the first 40 residues yielded channels with augmented responses to cold and menthol. The thermal threshold of activation of these mutants was shifted 2 °C to higher temperatures, and the menthol dose-response curve was displaced to lower concentrations. Site-directed mutagenesis screening revealed that single point mutations at positions Ser-26 or Ser-27 by proline caused a comparable increase in the responses to cold and menthol. Electrophysiological analysis of the S27P mutant revealed that the enhanced sensitivity to agonists is related to a leftward shift in the voltage dependence of activation, increasing the probability of channel openings at physiological membrane potentials. In addition, we found that the region encompassing positions 40–60 is a key element in the proper folding and assembly of TRPM8. Different deletions and mutations within this region rendered channels with an impaired function that are retained within the endoplasmic reticulum. Our results suggest a critical contribution of the initial region of the N-terminal domain of TRPM8 to thermal and chemical sensitivity and the proper biogenesis of this polymodal ion channel.

Ambient temperature sensing is fundamental for animal survival, allowing the rapid initiation of physiological and behavioral thermoregulatory responses. The detection and encoding of cold temperatures occurs in free nerve endings of cold-sensitive neurons in dorsal root and trigeminal ganglia (1–3). These endings express a large variety of ion channels, including transduction and voltage-dependent channels, which together shape the electrical response to different physical and chemical stimuli. Several members of the superfamily of transient receptor potential (TRP)[2] channels play a critical role in thermotransduction (4–6). Multiple findings indicate that the TRPM8 ion channel is the main molecular transducer for cold sensing in the somatosensory system (7–10); TRPM8 is an outwardly rectifying, Ca^{2+}-permeable, nonselective cation channel activated by cold temperatures and by several plant-derived and synthetic cooling compounds such as menthol and icilin (11, 12). TRPM8 is characterized by an unusually steep temperature sensitivity (13, 14). The mean temperature of TRPM8 activation is around 26 °C in heterologous expression systems and over 30 °C in mammalian cold-sensitive neurons (11, 12, 15, 16). The half-maximal effective concentration (EC_{50}) for TRPM8 activation by menthol is around 80 μM in heterologous expression systems (11). TRPM8 is also gated by voltage, although with a weak voltage dependence. At high temperatures, or in the absence of chemical agonists, activation requires stronger depolarizations (13, 17, 18). In contrast, cooling or menthol application shift the voltage-activation curve of TRPM8 toward more negative voltages, increasing the open probability of the channel at physiological membrane potentials (13, 18).

Functional TRPM8 channels are homotetramers (19–22) with six transmembrane domains and both the N and C termini located on the cytoplasmic side of the plasma membrane. Like

* This work was supported by Chilean Fondo Nacional de Ciencia y Tecnologia Grants 11130144 and 3110128 (to M. P.) and 1131064 (to R. M.), Comisión Nacional de Investigación Científica y Tecnológica Grant Anillo ACT-1113 (to R. M. and M. P.), and Spanish Ministerio de Ciencia e Innovación Projects SAF2010-14990 and SAF2013-4608-R (to F. V.).
[S] This article contains supplemental Table S1.
[1] Recipient of support from DICYT-VRIDEI of the University of Santiago de Chile. To whom correspondence should be addressed: Dept. de Biología, Facultad de Química y Biología, Universidad de Santiago de Chile, 9160000 Santiago, Chile. Tel.: 56-2-27181109; E-mail: maria.pertusa@usach.cl.

[2] The abbreviations used are: TRP, transient receptor potential; RIPA, radioimmune precipitation assay buffer; ER, endoplasmic reticulum; CFP, cyan fluorescent protein; MHR, melastatin homology regions; hTRPM8, human TRPM8; mTRPM, mouse TRPM; cTRPM, chicken TRPM; pF, picofarad; ANOVA, analysis of variance.

other ion channels, TRPM8 has distinct structural and functional modules (23). The C-terminal tail of this channel contains a TRP domain located in its proximal part (19, 24). Within this domain, neutralization of lysines and arginines greatly decreases the sensitivity of TRPM8 to phosphatidylinositol bisphosphate, a key modulator of the channel function (25). Another important region within the C terminus is a coiled-coil motif formed by the last 40 residues. Although some studies suggest a critical role of this domain in the oligomerization of the protein (22, 26), another study indicates that tetramerization is still possible in C-terminal deletion mutants, although channel function is impaired (27). Regarding the transmembrane domains and their connecting loops, charge-neutralizing mutations in transmembrane segment 4 (S4) and the S4-S5 linker of TRPM8 modify its voltage sensitivity (28). The pore module consists of the S5 and S6 domains and the interconnecting loop, where the pore filter is located (29). TRPM8 is also *N*-glycosylated in this extracellular loop, specifically on the Asn residue at position 934, near the pore (26, 30). This post-translational modification, also observed in native channels (31, 32), plays a role in localizing TRPM8 channels on lipid rafts (31), and it is an important determinant of TRPM8 sensitivity to chemical and thermal stimuli (32). Most of TRPM8-binding sites for chemical agonists and antagonists have been mapped on transmembrane domains. For example, position Tyr-745 in S2 is involved in channel activation by menthol (33), and it also mediates the inhibition by SKF96365 (34). Mutations in the S4 and in the S4-S5 linker also affect menthol affinity (20, 28), and the effect of the artificial cooling compound icilin requires the residues Asn-799, Asp-802, and Gly-805 within S3 (35).

In rodents and humans, the intracellular N-terminal domain of TRPM8 is highly conserved and composed of the first 693 amino acids of the protein. This domain contains four stretches of amino acids that share some sequence similarity with other members of the TRPM family, called melastatin homology regions (MHR) (19, 36), that do not represent known structural motifs. Nowadays, the role of the N terminus in TRPM8 function remains poorly understood. A quaternary structure model for TRPM8 ion channels postulates that the MHR regions may be involved in stabilization of the tetramer (37). Upstream of the first MHR, TRPM8 contains a 116-amino acid sequence where in a previous study (27) two important observations were made. First, the authors showed that the first 39 amino acids are dispensable for proper channel function. Second, they found that a stretch encompassing residues 40–86 was needed for the proper trafficking of TRPM8 to the plasma membrane (27).

Some TRP channels display splice variants that lead to alterations in channel activity and/or subcellular distribution (38). Similarly, the *Trpm8* gene encodes for several isoforms that are expressed in lung epithelia (39) and in human prostate cancer cells (40, 41). Three TRPM8 splice variants have been identified in prostate cancer cell lines as follows: two short N terminus-derived isoforms that lack all transmembrane domains (40), and a third one with a truncation in the initial N-terminal domain (41). The two short isoforms, through interaction with the full-length channel, cause a reduction in the cold response of TRPM8 (40). The functionality of the third splice variant is still unclear (41). Thus, exploring the role of the large N terminus in TRPM8 activity remains an important step toward clarifying the contribution of this third isoform in normal and pathophysiological conditions.

With the aforesaid precedents, the main goal of our study was to investigate the role of the initial N-terminal domain in the biogenesis, trafficking, and function of TRPM8. Combining mutagenesis and design of chimeric constructs with functional assays of channel activity, we identified a minimal region required for proper channel function and single residues strongly modulating the gating of the channel by physiological and chemical agonists.

EXPERIMENTAL PROCEDURES

Molecular Biology and Site-directed Mutagenesis—The full-length cDNA encoding mouse TRPM8 in pcDNA5, human TRPM8 in pcDNA3, chicken TRPM8 in pcDNA3, and mouse TRPM2 in pCIneo vector were kindly provided by Ardem Patapoutian, Veit Flockerzi, David Julius, and Yasuo Mori, respectively. The nonfunctional TRPV1 (ΔTRPV1) and the ER-red fluorescent protein marker used in this study were contributed by A. F. Montiel and J. G. Sancho, respectively. TRPM8 point mutants were obtained by site-directed mutagenesis, deletions by inverse PCR, and chimeras by overlap extension PCR. In all of these techniques, we used Pfu Turbo polymerase (Stratagene). The primers necessary for these manipulations are detailed in supplemental Table 1. The mutated TRPM8 sequences were subcloned in pcDNA3 Myc (Invitrogen), and in the case of fusion proteins with the YFP and CFP added to the C terminus, the TRPM8 constructs were subcloned in pEYFP-N1 and pECFP-N1 (Clontech). Before use, all the constructs were verified by DNA sequencing.

Western Blot and Immunocytochemistry—HEK293 cells, transiently transfected with wild type or mutant TRPM8 channels, were washed with phosphate-buffered saline (PBS) and solubilized in RIPA buffer (PBS at pH 7.4, 0.1% (w/v) SDS, 1% (v/v) Nonidet P-40, 0.5% (w/v) sodium deoxycholate) supplemented with a mixture of protease inhibitors (Thermo Scientific). Lysates were centrifuged at 10,500 × *g* for 15 min at 4 °C, and the protein concentration in the supernatant was measured with the BCA protein assay reagent (Thermo Scientific). Equal amounts of protein for each condition (15–30 μg) were denatured at 95 °C for 5 min, loaded onto a 7.5% SDS-polyacrylamide gel, and electrophoresed. Proteins were transferred to a nitrocellulose membrane, blocked with 10% skim milk in PBS, incubated with antibodies against the c-Myc epitope and GAPDH (Sigma), and diluted to 1:3000 and 1:10,000, respectively, in T-PBS. Horseradish peroxidase (HRP)-coupled anti-rabbit secondary antibodies (Sigma) were used at a final concentration of 1:2000 for detection, and the signal was developed with a SuperSignal West Pico chemiluminescence kit (Thermo Scientific). The immunoreactive bands were digitized, and a densitometry analysis was performed using ImageJ software (42). Band intensities from at least three independent experiments were quantified and normalized to GAPDH expression as protein loading control.

For immunocytochemistry, glass coverslips with seeded cells were fixed in 4% fresh paraformaldehyde for 10 min and washed twice with PBS. After washing, the cells were blocked for 1 h

with a PBS solution containing 1% BSA and 0.1% Triton X-100. Primary polyclonal anti-Myc (Sigma) was diluted to 1:2000 in blocking solution and incubated at 4 °C overnight. After washing three times with PBS, the secondary antibody, Alexa Fluor 488 anti-rabbit (Invitrogen), was added for 2 h at 1:2000 dilution. Coverslips with stained cells were mounted in a fluorescent antifading medium (SouthernBiotech). Stained cells were visualized with a Zeiss confocal laser scanning microscope model LSM 510 (Carl Zeiss) equipped with 488- and 543-nm laser lines. Image analysis was performed with LSM Lite software (Carl Zeiss).

Co-immunoprecipitation—HEK293 cells were transiently transfected in a 60-mm dish and harvested in 500 μl of RIPA buffer supplemented with a protease inhibitors mixture. Particulate material was removed by centrifugation for 20 min at 10,500 $\times$ *g* and 4 °C. Δ41–57 TRPM8-YFP and Δ1059–1104 TRPM8-YFP proteins were immunoprecipitated using a 1:500 anti-GFP antibody (Sigma) for 16 h at 4 °C, followed by 2 h at room temperature with protein G-Sepharose (Roche Applied Science). Immunoprecipitates were washed three times with 1 ml of RIPA buffer. Finally, the whole extract and the immunoprecipitates were subjected to SDS-gel electrophoresis (8% polyacrylamide) and blotted on nitrocellulose. Immunodetection was carried out using rabbit anti-TRPM8 at 1:500 (31).

Cell Culture and Transfection—HEK293 cells were plated in 24-well dishes at 1×10^5 cells/well and transiently transfected with 1 μg of indicated DNA and Lipofectamine 2000 (Invitrogen), following the manufacturer's indications. At 48 h post-transfection, protein expression analysis and calcium imaging experiments were performed.

Fluorescence Ca^{2+} Imaging—HEK293 cells co-transfected for 48 h with 1 μg of TRPM8 construct and 0.25 μg of a fluorescent reporter (*e.g.* GFP) were loaded with 5 μM Fura-2AM (Invitrogen) in standard extracellular solution (in mM): 140 NaCl, 3 KCl, 1.3 $MgCl_2$, 2.4 $CaCl_2$, 10 glucose, and 10 HEPES, pH 7.4, adjusted with NaOH (297 mosM/kg) supplemented with 0.02% pluronic acid (Invitrogen) for 45 min at 37 °C in darkness. Fluorescence measurements were made with an inverted Nikon Eclipse Ti microscope fitted with a 12-bit cooled ORCA C8484-03G02 CCD camera (Hamamatsu). Fura-2 was excited at 340 and 380 nm with a polychrome V monochromator (Till Photonics), with exposure times of 30 ms, and the emitted fluorescence was filtered with a 510-nm long pass filter. Calibrated ratios sampled every 2 s were displayed on line with HCImage version 1.2 software (Hamamatsu). Bath temperature (see below for details) was recorded simultaneously with an IT-18 T-thermocouple connected to a Physitemp BAT-12 microprobe thermometer (Physitemp Instruments) and digitized with an Axon Digidata 1440A AD converter running Clampex 10 software (Molecular Devices). Threshold temperature values for $[Ca^{2+}]_i$ elevation were estimated as in Ref. 17 by linearly interpolating the temperature at the midpoint between the last base-line point and the first point where a rise in $[Ca^{2+}]_i$ deviated by at least four times the standard deviation of the base line.

Fluorescence Resonance Energy Transfer (FRET)—FRET efficiency was evaluated with the "acceptor photobleaching" (donor dequenching) method. Measurements were carried out with a laser scanning confocal microscope (model TCS SP2 AOBS) using confocal software (Leica Microsystems). Experiments were performed on transfected HEK293 cells fixed in 4% paraformaldehyde in PBS. Single-cell FRET efficiencies were obtained after monitoring the increase in the CFP (FRET donor) fluorescence emission during selective YFP (FRET acceptor) photobleaching (43, 44). FRET efficiency was calculated as the percentage increase in CFP emission after YFP photobleaching by using the following formula: percent FRET (%) = ((CFPpost − CFPpre)/CFPpre) × 100, where CFPpost is the CFP emission after YFP photobleaching, and CFPpre is the CFP emission before YFP photobleaching.

Electrophysiological Recordings—Whole-cell voltage clamp recordings in transfected HEK293 cells were performed simultaneously with temperature recordings. Standard patch pipettes (3–5 megohms) were made of borosilicate glass capillaries (Harvard Apparatus Ltd.) and contained (in mM) the following: 130 CsCl, 1 EGTA, 10 HEPES, 4 ATPMg, and 0.4 GTPNa, adjusted to pH 7.4 with CsOH (280 mosM/kg). The bath solution was the same as in the calcium imaging experiments. Current signals were recorded with an Axopatch 200B patch clamp amplifier (Molecular Devices). Stimulus delivery and data acquisition were performed using pCLAMP10 software (Molecular Devices).

To estimate the shifts in the voltage dependence of TRPM8 activation, current-voltage (*I-V*) relationships obtained from repetitive (0.2 Hz) voltage ramps (−100 to +180 mV, with a slope of 200 mV/s) were fitted with a function that combines a linear conductance multiplied by a Boltzmann activation term (45) shown in Equation 1,

$$I = g \times (V - E_{rev})/(1+\exp((V_{1/2} - V)/s)) \qquad \text{(Eq. 1)}$$

where g is the whole-cell conductance; E_{rev} is the reversal potential of the current; $V_{1/2}$ is the potential for half-maximal activation; and s is the slope factor. The assumption of a linear conductance is based on the observation by Voets *et al.* (18) that open TRPM8 channels exhibit ohmic *I-V* dependence.

Temperature Stimulation—Coverslips with cultured cells were placed in a microchamber and continuously perfused with solutions warmed to ~34 °C. The temperature was adjusted with a water-cooled computer-controlled Peltier device placed at the inlet of the recording chamber and controlled by a feedback device. Cold sensitivity was investigated with temperature drops from 34 to 18 °C.

RESULTS

Distal N-terminal Region Encompassing Positions 40–60 Is Important for Normal Biogenesis of TRPM8—Previous work showed that deletion of the first 86 amino acids in the N-terminal domain produces a retention of TRPM8 in the ER and/or Golgi compartments (27). The abnormal intracellular retention of this mutant may be explained in two different ways as follows: the removal of a trafficking signal encoded in this region may prevent proper targeting of the channel to the plasma membrane (46), or defects in proper channel assembly may be detected by a quality control mechanism leading to its retention within the ER (47). To discriminate between these two possibil-

ities, we used calcium imaging to assess the functionality of the mutant. This technique has been used to monitor TRPM8 activity localized in both the plasma membrane and the ER compartment (48–50). Indeed, we showed previously that, in transfected HEK293 cells, functional TRPM8 activity from the ER can be detected by calcium imaging when cold and menthol stimuli are applied simultaneously (*i.e.* using a saturating stimulus) (32). Therefore, in the hypothetical case that TRPM8 mutant subunits are properly folded and the homotetramer is correctly assembled, we should observe a response to a combined cold and menthol stimulation even if the channel is mainly localized in the ER, suggesting that the deletion would be affecting primarily the normal trafficking of the channel.

In Fig. 1*A*, we show a schematic representation of some of the deletions and chimeras used in this work, based on mTRPM8-myc (mM8-myc) whose responses are identical to those of mTRPM8 (data not shown). First, we generated channels with deletions in the 40–60-residue region of mM8-myc (Δ41–57) and examined four different aspects as follows: the expression of the protein by Western blot, its degree of glycosylation, the subcellular distribution, and the channel activation by cold and menthol. The Δ41–57 construct showed an expected band of ~128 kDa (Fig. 1*B*), with clear differences in its glycosylation state compared with wild type channels. TRPM8 is *N*-glycosylated at position Asn-934 (26, 30), and the molecular mass of the fully glycosylated monomer exceeds the 130 kDa predicted by the amino acid sequence. This higher molecular weight band represents the mature *N*-glycosylation form, which is generated during the transit of the channel through the Golgi apparatus (32). As shown in Fig. 1*B*, the Δ41–57 deletion lacks the upper band corresponding to the fully glycosylated state. Because the *N*-glycosylation site should not be affected by this deletion, the lack of glycosylation suggests that this mutant is retained in the ER. Immunocytochemistry experiments corroborated this hypothesis. The fully functional mM8-myc appears to be largely distributed in vesicles (Fig. 1*C*), with a pattern similar to that displayed by other TRP channels when they are overexpressed in HEK293 cells (51). In contrast, the Δ41–57 deletion displays a substantial overlap with an ER marker (Fig. 1*C*). Besides changes in the subcellular distribution pattern, Δ41–57 also displays a complete loss of response to cold, menthol (100 μM), or to the application of both stimuli simultaneously (Fig. 1*D*). The impaired activity, together with the ER retention, suggests that this deletion produces defects in proper folding and assembly of the channel that are detected by quality control systems preventing its exit from the ER. To better delineate the sequence responsible for this phenotype, we performed two smaller deletions within this region, Δ41–48 and Δ49–57. Both of them display the same phenotype as the Δ41–57 truncation, *i.e.* absence of mature glycosylation, lack of response to cold and menthol, and retention in the ER (see Fig. 1*A* for a summary of the functional phenotypes).

Our next challenge was to identify the key residue(s) responsible for this nonfunctional phenotype. Considering that the closest relative of TRPM8 is TRPM2 and that specifically the 40–60-residue region is moderately well conserved (see Fig. 1*E*), our intention was to rescue the phenotype displayed by the deletion, replacing the 60 first amino acids by the homolog sequence of TRPM2 (1–76 M2/M8) (Fig. 1*E*). However, the resulting chimera also exhibited a complete loss of activity and ER retention. Therefore, we reasoned that some nonconserved positions may be critical for the proper folding and assembly of TRPM8. We swapped stretches of 10 amino acids within the 40–60-residue region with the related sequence of TRPM2. The sequence of these chimeras is detailed in Fig. 1*E*. The 40–49 M2/M8 substitution did not affect the biochemical and functional properties of TRPM8 significantly (Fig. 1, *A* and *B*), although the two channels share only three of the 10 amino acids within this region (Fig. 1*E*). In contrast, the 50–59 M2/M8 chimera showed a completely novel phenotype. Immunocytochemistry experiments showed that this mutant channel is mainly localized in the ER. Accordingly, the protein lacks mature glycosylation (see Fig. 1*B*). However, unlike the other nonfunctional mutants reported that did not exhibit any responses to cold and menthol, almost 50% of cells transfected with this chimera showed a detectable response when both agonists were applied simultaneously (Fig. 1*D*). TRPM8 and TRPM2 present a marked conservation in the 50–59-residue region of TRPM8, with differences only in four positions: R52(K), F56(Y), T58(V), and R59(E) (see Fig. 1*E* for sequence comparison). Experiments with the double mutant T58V/R59E indicated that these two residues are the main contributors to the phenotype observed in the 50–59 M2/M8 chimera (see Fig. 1, *A* and *B*). These results suggest an important role of Thr-58 and Arg-59 in the proper biogenesis and functionality of TRPM8.

In addition to these constructs, we also studied a human splice variant of TRPM8 (hTRPM8b), which is expressed in prostate cancer cell lines such as LNCaP, DU-145, and PC-3 (49). This splice variant is characterized by an alternative start codon that renders a protein without the first 65 amino acids (41). To this end, we created a truncated mutant of hTRPM8-myc that mimics the endogenous splice variant (hTRPM8b). This protein lacks the mature glycosylation (see Fig. 1*B*), is mainly localized in the ER compartment, and exhibits no response to cold and menthol (see summary in Fig. 1*A*), indicating that it is highly unlikely that this splice variant can form an active homotetrameric channel by itself in the tissues where it is expressed.

50–59 M2/M8 Channels Are Present in the Plasma Membrane and Display Impaired Activity—To study in more detail the phenotype displayed by the 50–59 M2/M8 chimera, we performed experiments in calcium-free solutions. The main goal of this approach was to determine whether the calcium responses observed in this mutant are due to the presence of channels in the ER, as its main subcellular distribution suggests (see Fig. 1*A*). As reported previously (32), calcium-free conditions revealed a small contribution of TRPM8 channels located in the ER compartment in the whole response to the saturating (cold plus menthol) stimulus (Fig. 2, *A* and *B*). Surprisingly, despite the main ER retention displayed by the 50–59 M2/M8 construct, the full response exhibited by this mutant to the combined stimulus required extracellular calcium, indicating that the calcium rise did not depend on channels in the ER and suggesting that some of these mutant channels are able to reach the plasma membrane. To confirm the presence of this chimera

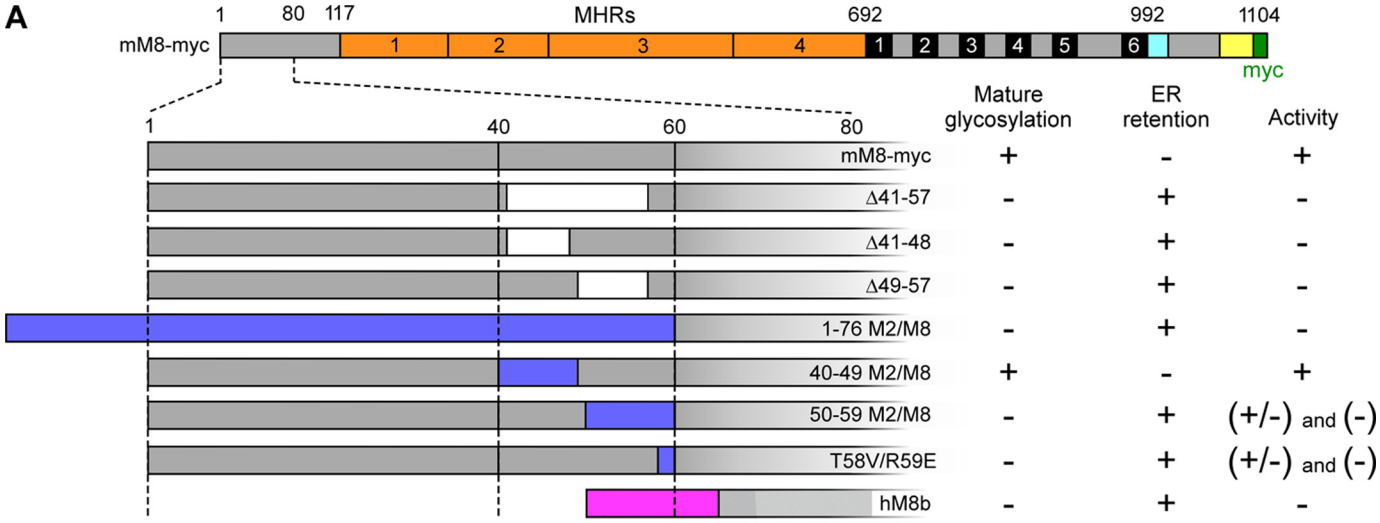

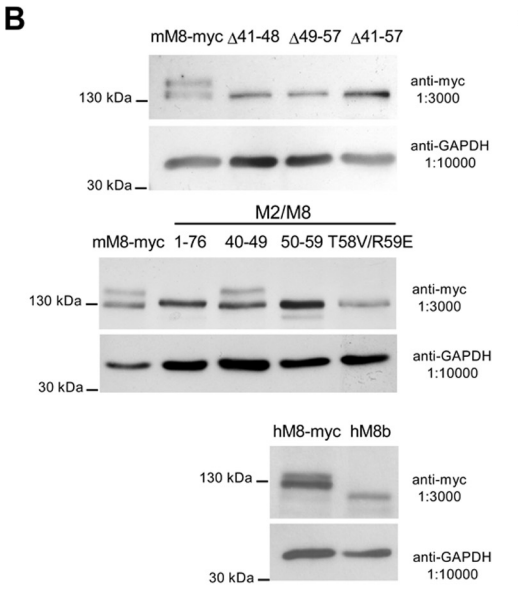

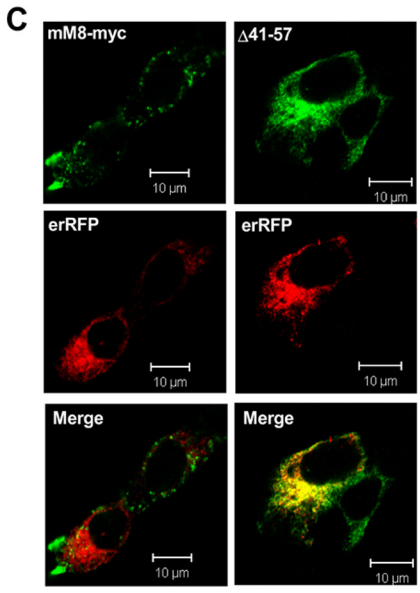

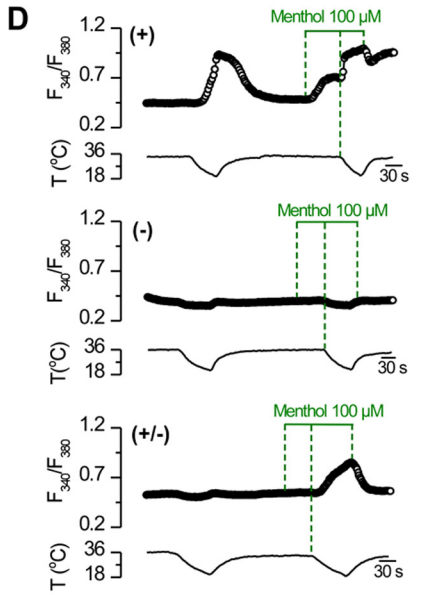

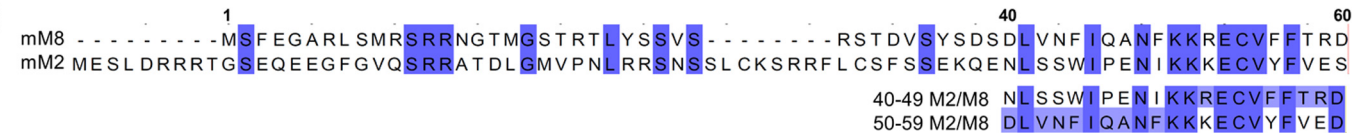

FIGURE 1. **Region encompassing positions 40–60 in the N terminus of TRPM8 is critical for channel biogenesis and activity.** *A,* primary structure of TRPM8 is shown in the *upper panel* (the MHRs in *orange*, the six transmembrane domains in *black*, the TRP domain in *cyan*, the coiled-coil region in *yellow*, and the Myc epitope in *green*). The *bottom panel* depicts a schematic of the deletions, chimeras, and splice variants used in the first part of this study with a summary of the biochemical and functional features displayed by each construct. All the constructs were obtained using mTRPM8-myc (mM8-myc) as template, except hTRPM8b (*hM8b*) which is based on hTRPM8-myc. We evaluated the presence of mature glycosylation by Western blotting, retention in ER by co-localization with an ER marker, and functional activity by calcium imaging. *B,* Western blots of cell lysates from HEK293 cells transfected with different deletions and chimeras of TRPM8-myc probed with an anti-Myc antibody. In these experiments GAPDH was used as a loading control. *C,* immunocytochemistry of HEK293 cells co-transfected with TRPM8 and an ER fluorescent marker. *Upper panels* show immunofluorescence staining of mM8-myc and the Δ41–57 deletion. *Middle panels* show the ER marker that consists of the recognition sequence of calreticulin fused to red fluorescent protein. *Lower panels* show the merger of these images. *D,* representative intracellular calcium imaging traces showing responses to cold, to 100 μM menthol, and to a combined stimulus of cold in the presence of 100 μM menthol. The + type corresponds to the canonical response of a HEK293 cell transfected with mM8-myc. The − type corresponds to a cell transfected with the 1–76M2/M8 chimera, a typical nonfunctional channel. The +/− type shows responses only to a combined stimulus of cold and menthol. This type of response is detected in about 50% of the cells with the 50–59 M2/M8 chimera. *E,* alignment of the amino acid sequences of mouse TRPM8 and mouse TRPM2, using Clustal Omega and Jalview. The numbers correspond to the residues in mTRPM8. In the *bottom panel*, sequences of chimeras 40–49 M2/M8 and 50–59 M2/M8 are shown; shown in *white* are residues that are different from mTRPM8.

on the cell surface, and to further study the biophysical properties of this mutant, we performed electrophysiological experiments. HEK293 cells transfected with mM8-myc and 50–59 M2/M8 construct were held at −60 mV, and channel activation was probed with 1400-ms duration voltage ramps from −100 to +180 mV, applied at a frequency of 0.2 Hz, to obtain the *I-V* relationships for both channels. Cells were stimulated using the same protocol as in calcium imaging experiments, *i.e.* sequen-

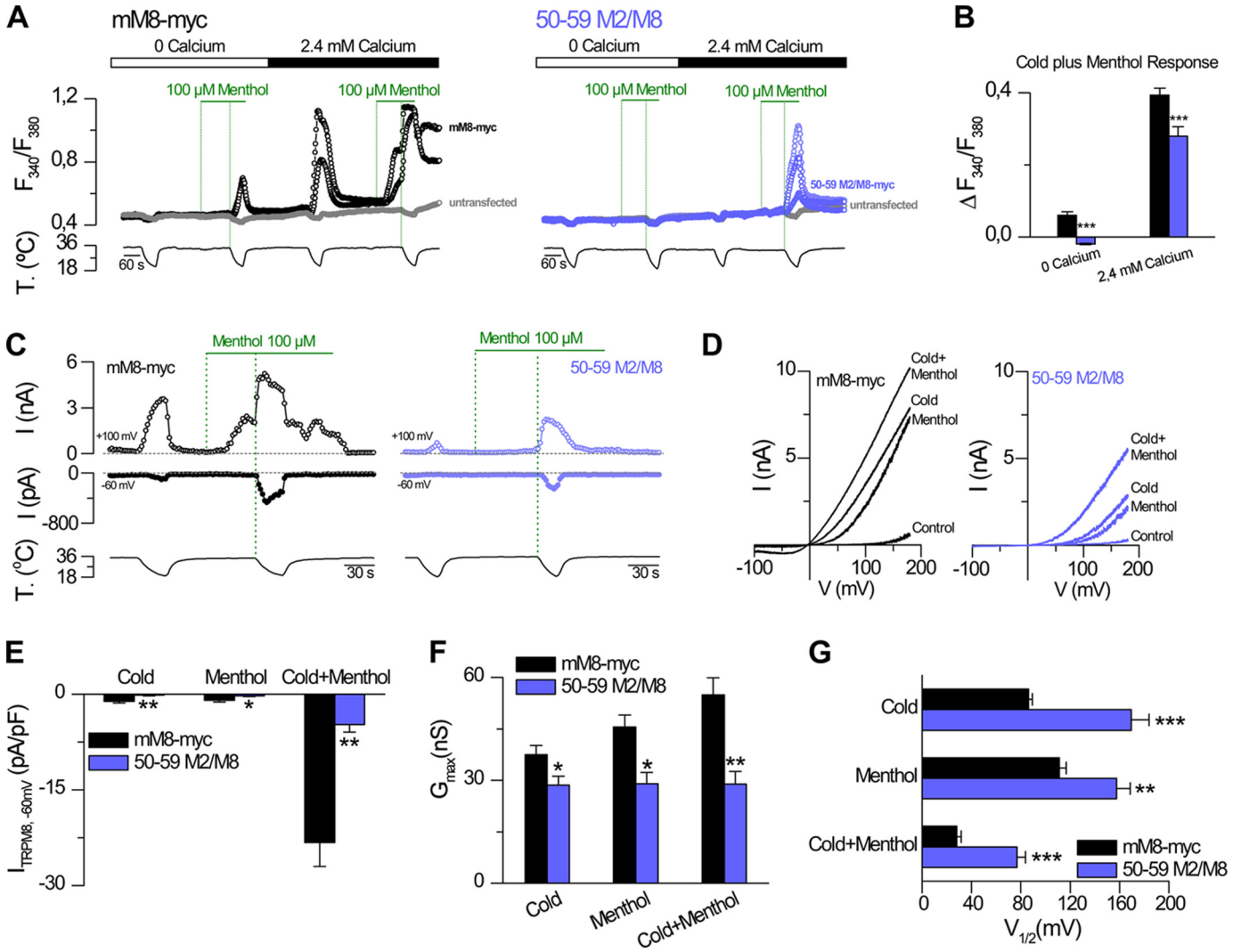

FIGURE 2. **50–59 M2/M8 construct shows impaired activity resulting from a reduction in the surface expression and alterations in its biophysical properties.** *A,* representative intracellular calcium imaging traces showing responses to cold and 100 μM menthol in cells expressing mM8-myc (*black*) or 50–59 M2/M8 (*purple*) and in nontransfected HEK293 cells (*gray*). Note the lack of response to cold or menthol in untransfected cells. The protocol was performed under normal (2.4 mM) and zero external Ca^{2+} conditions. *B,* summary histogram of the results obtained in cold plus menthol conditions in the experimental protocol shown in *A*. The intracellular calcium increases for mM8-myc, and 50–59 M2/M8 were compared using an unpaired Student *t* test: ***, $p < 0.001$; mM8-myc, $n = 51$; 50–59 M2/M8, $n = 36$. *C,* representative recording of whole-cell currents measured at +100 and −60 mV in a HEK293 cell transfected with mM8-myc (*black*) or 50–59 M2/M8 (*purple*) channels during a temperature drop, the application of 100 μM menthol at 34 °C, and a second temperature reduction during application of 100 μM menthol. Whole-cell capacitance of mM8-myc and 50–59 M2/M8-expressing cells (*C* and *D*) was 14 and 12 pF, respectively. *D,* current-voltage relationships at 34 °C in control solution (*control*), at 20 °C in control solution (*cold*), at 34 °C in control solution supplemented with 100 μM menthol (*menthol*), and at 20 °C in the presence of 100 μM menthol (*cold plus menthol*) of the same cells as in *C*. *Traces* on the *left panel* are current-voltage relationships of mM8-myc transfected HEK293 cells (*black*). On the *right panel*, traces correspond to the 50–59 M2/M8 construct (*purple*). *E, bar graph* summary of the mean ± S.E. values of maximal current density at −60 mV under the different conditions tested. *F* and *G, bar graph* summary of the mean values of G_{max} and $V_{1/2}$ obtained from the fits of the currents to Equation 1. *Black bars* correspond to mM8-myc and *purple bars* to 50–59 M2/M8 channels. Recordings from wild type and mutant channels were always interlaced on the same day. Statistical significance was assessed with a two-tailed unpaired Student *t* test: *, $p < 0.05$; **, $p < 0.01$; ***, $p < 0.001$, $n > 6$ cells for each condition.

tial applications of cold, menthol, and cold in the presence of menthol (Fig. 2, *C* and *D*). At −60 mV, cells expressing the 50–59 M2/M8 channel displayed an almost undetectable response to cold or 100 μM menthol and a marked reduction of the response to their combined application compared with the mM8-myc channel (Fig. 2*E*). This result can be explained by a change in the total number of channels in the plasma membrane and/or alteration in their biophysical properties. To clarify this point, we estimated the maximal conductance (G_{max}), the voltage at the midpoint of activation ($V_{½}$), and the voltage dependence (slope factor (*s*)) for both channels. The current traces obtained using the voltage ramp protocol were fitted with a Boltzmann linear function (see "Experimental Procedures"), and the analysis of the G_{max} value under the cold plus menthol condition (a condition that activates all the channels in the plasma membrane) revealed a reduction of this value to one-half, suggesting that the presence of this construct in the plasma membrane is decreased (Fig. 2*F*). This chimera also showed an important shift in the $V_{½}$ of activation toward more positive potentials compared with the mM8-myc channel (Fig. 2*G*), which also contributed to the reduction in the responses observed in the 50–59 M2/M8 mutant. No change in slope factor was observed (41 ± 1 mV^{-1}, mM8-myc *versus* 37 ± 2 mV^{-1}, 50–59 M2/M8, cold condition; 40 ± 1 mV^{-1}, mM8-

myc *versus* 36 ± 2 mV^{-1}, 50–59 M2/M8, menthol condition; 47 ± 2 mV^{-1}, mM8-myc *versus* 47 ± 2 mV^{-1}, 50–59 M2/M8, cold plus menthol condition). In conclusion, the phenotype displayed by this chimera is the result of two factors as follows: an apparent reduction in the number of channels that reach the plasma membrane, and a marked impairment in their gating. Altogether, these results corroborated the importance of the N terminus in the generation of a fully functional TRPM8 channel.

FRET Experiments Reveal the Relevance of the N Terminus in the Quaternary Structure of TRPM8—Based on the expression pattern and functional deficits presented above, we hypothesized that the region between positions 40 and 60 of the N terminus may be a key element in the proper assembly of the tetrameric protein (*i.e.* quaternary structure of TRPM8). Thus, to explore whether a deletion within this region could affect the interaction between subunits, we performed co-immunoprecipitation experiments. To this end, we used a Δ41–57 deletion construct fused with YFP in the C terminus, co-expressed with the wild type mTRPM8 channel in HEK293 cells. We chose the Δ41–57 construct because, unlike 50–59 M2/M8, this deletion completely abrogates TRPM8 activity and is likely to produce larger changes on the quaternary structure of the channel. We also evaluated a Δ1059–1104 construct characterized by the lack of the coiled-coil domain in the C terminus that drives tetramerization of the TRPM8 and has the same phenotype as the Δ41–57 deletion (prevention of mature glycosylation and no function (26)). As a negative control, we used a co-transfection of mTRPM8 with a nonfunctional version of ΔTRPV1 (52). In Fig. 3*A*, the *left panel* shows total cell lysates, *i.e.* the 140- and 130-kDa bands correspond to wild type TRPM8 (glycosylated and unglycosylated), whereas the band with a molecular mass of ~170 kDa corresponds to the two deletions of TRPM8 fused with YFP. In Fig. 3*A*, *right panel*, the immunoprecipitation results show that neither of the deletions (Δ1059–1104 and Δ41–57) prevented the interaction of the mutant constructs with the wild type subunits of mTRPM8. It is noteworthy that the immunoprecipitated mTRPM8 corresponds to the unglycosylated and/or immature form of *N*-glycosylation (Fig. 3*A*), suggesting that the wild type subunits that immunoprecipitate with deletion subunits are also retained in the ER. Interestingly, the Δ1059–1104 construct, despite the reported defects in tetramerization (22, 26), is able to interact with wild type subunits.

To further study the role of the 40–60-residue region in the quaternary structure of TRPM8, we evaluated the interaction of the different TRPM8 subunits using FRET. To this end, we used a TRPM8-CFP construct co-transfected with four different constructs as follows: TRPM8-YFP, Δ5–39 TRPM8-YFP, Δ41–57 TRPM8-YFP, and Δ1059–1104 TRPM8-YFP (both CFP and YFP were added to the C terminus of TRPM8). As summarized in Fig. 3*B*, co-transfection of both full-length channel subunits yielded a FRET efficiency of ~23%. A similar value was found using the Δ5–39 deletion as a YFP pair. However, the use of Δ1059–1104 TRPM8-YFP and Δ41–57 TRPM8 YFP constructs dropped the FRET efficiency to less than 5%, suggesting that these deletions cause an alteration in the interaction among different subunits (Fig. 3*B*). These results suggest

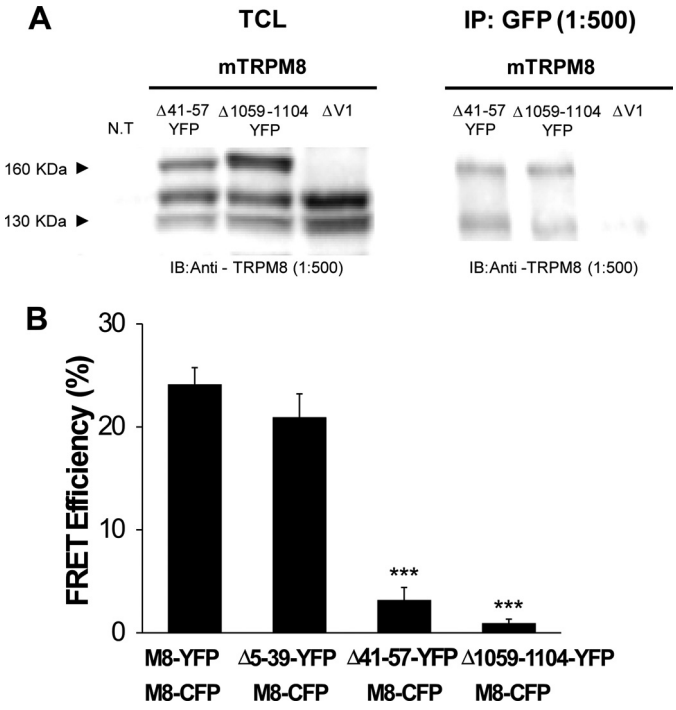

FIGURE 3. **Analysis of the biochemical and functional interaction of TRPM8 subunits with truncations in the N- and C-terminal domains.** *A,* co-immunoprecipitation of mTRPM8 co-expressed with different TRPM8-YFP deletions. A nonfunctional ΔTRPV1 construct was used as a negative control. *Left blot* shows total cell lysates (*TCL*) probed with anti-TRPM8 antibody. The *right blot* shows TRPM8 constructs immunoprecipitated (*IP*) with GFP antibody and immunoblotted (*IB*) with anti-TRPM8. *B,* FRET efficiencies determined between different TRPM8 constructs with YFP and CFP conjugated on their C terminus ($n = 8$, for each construct, obtained in two independent experiments). FRET efficiencies were compared using a one-way ANOVA test in combination with Dunnett's post hoc test: ***, $p < 0.001$ with respect to the TRPM8-YFP and TRPM8-CFP pair.

that, in addition to the coiled-coil domain in the C terminus, this small region in the N-terminal domain is also important in the proper folding and assembly of TRPM8.

First 40 Amino Acids in the N Terminus Dampen the Sensitivity of TRPM8 to Cold and Menthol—To rule out that any given deletion within the initial N-terminal domain could yield nonfunctional channels, we studied a deletion encompassing positions 4–40 of mTRPM8-myc (Δ5–39). In agreement with previous results (27), this deletion produced functional channels, activated by cold and menthol (Fig. 4). Moreover, calcium imaging experiments indicated that this mutation causes a marked enhancement in the responses of TRPM8 to both agonists, as shown in Fig. 4, *A* and *B*. To characterize this deletion further, we used a stimulation protocol consisting of a cold ramp followed by the application of increasing concentrations of menthol (10–300 μM) and a final cold ramp in the presence of 300 μM menthol (Fig. 4*C*). These experiments revealed that the deletion shifts the temperature threshold of activation almost 2 °C to warmer temperatures compared with the control channel (mM8-myc, 25.2 ± 0.1 °C; Δ5–39, 27.0 ± 0.1 °C) and yielded a lower EC_{50} value for menthol activation (mM8-myc, 127 ± 7 μM; Δ5–39, 46 ± 17 μM, $p < 0.001$, Fisher's exact test), demonstrating that the absence of this region causes an increase in the sensitivity of the channel to agonists (Fig. 4, *D–F*). A similar result was obtained when the first 40 amino

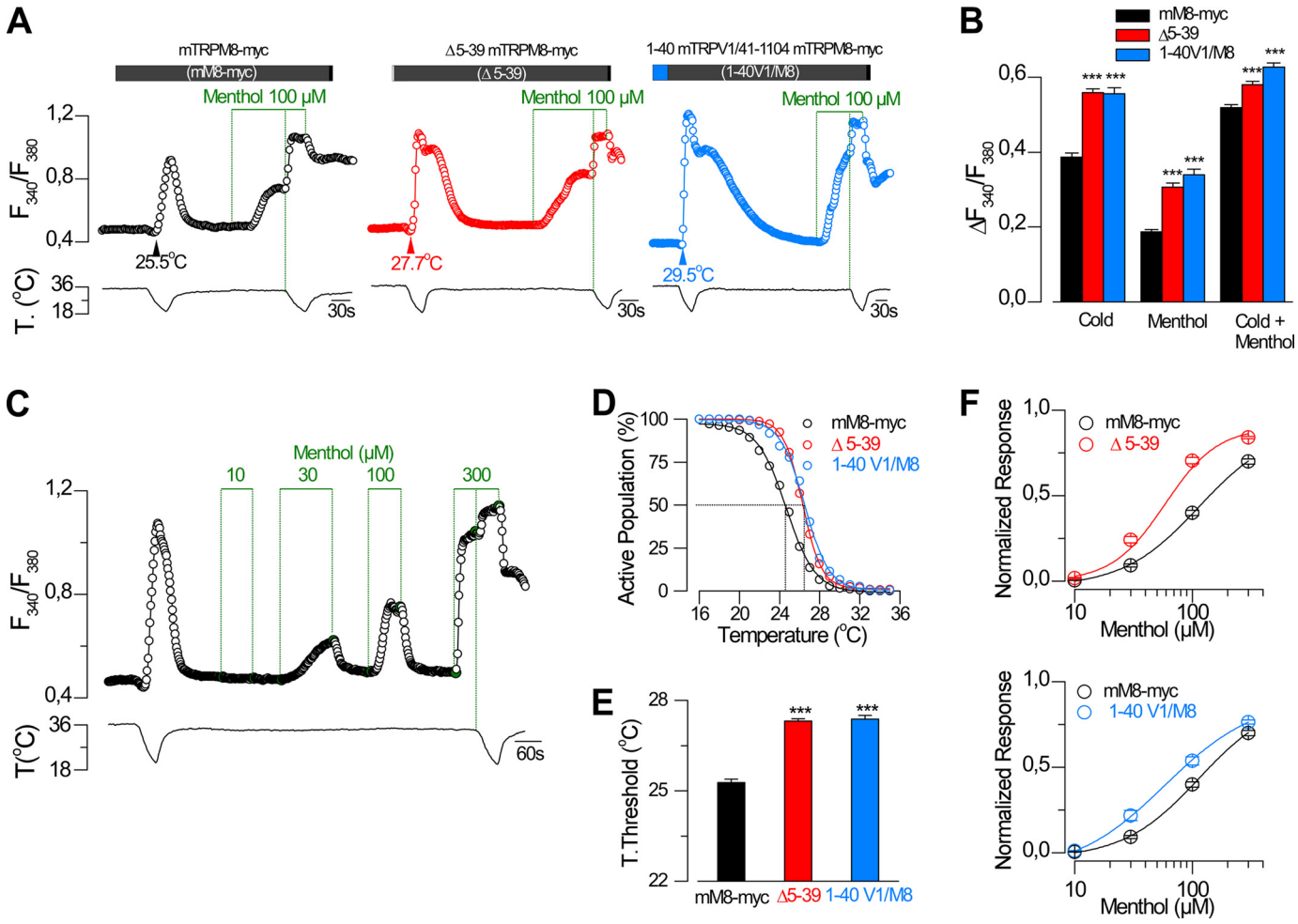

FIGURE 4. **Region containing the first 40 amino acids in the N-terminal domain modulates TRPM8 sensitivity to cold and menthol.** *A,* representative intracellular calcium imaging traces showing responses to cold and 100 μM menthol in cells expressing TRPM8-myc (*mM8-myc, black, left panel*), Δ5–39 TRPM8-myc (*Δ5–39, red, middle panel*), and a chimera 1–40 mTRPV1/41–1104 mTRPM8-myc (*1–40 V1/M8, blue right panel*). *B,* summary histogram of the results obtained for the experimental protocol in *A*. Statistical significance was assessed with a one-way ANOVA test in combination with a Dunnett's post hoc test; ratios are different (***, $p < 0.001$) with respect to mM8-myc, $n = 458$; Δ5–39, $n = 334$; 1–40 V1/M8, $n = 223$. *C,* time course of $[Ca^{2+}]_i$ response during cooling ramps and applications of menthol at different concentrations in a HEK293 cell co-transfected with mTRPM8-myc and GFP. *D,* percentage of active population recruited during a cooling ramp in HEK293 cells transfected with mM8-myc, Δ5–39, and 1–40V1/M8 channels. *E,* histogram of mean ± S.E. temperature thresholds exhibited by HEK293 cells transfected with mM8-myc ($n = 548$), Δ5–39 ($n = 512$), and 1–40V1/M8 ($n = 336$). Temperature thresholds were compared using a one-way ANOVA test in combination with a Dunnett's post hoc test: ***, $p < 0.001$ with respect to mM8-myc. *F,* dose-response curves of responses to menthol in transfected HEK293 cells. *Upper panel* shows the comparison of mM8-myc with Δ5–39. The *solid lines* represent fits to the Hill equation that yielded an EC_{50} of 127 ± 7 μM for mM8-myc and 46 ± 17 μM for Δ5–39 (mM8-myc, $n = 93$; Δ5–39, $n = 180$). Responses were normalized to the amplitude obtained with maximal stimulation (300 μM menthol plus cold). *Lower panel* shows the comparison of mM8-myc with 1–40V1/M8 construct in simultaneous experiments (1–40V1/M8, $n = 103$; EC_{50} of 60 ± 1 μM). Recordings from wild type and mutant channels were interlaced on the same day.

acids of TRPM8 were substituted by the corresponding region of mouse TRPV1, a heat-activated thermo-TRP (53) (1–40V1/M8). In this case, the temperature threshold and the EC_{50} value for menthol were 27.4 ± 0.1 °C and 60 ± 1 μM, respectively (Fig. 4, *E* and *F*). These results suggest that the region encompassing the first 40 amino acids in the N terminus may be involved in regulating the activation properties and sensitivity of TRPM8 to cold and menthol.

Our next goal was to define the minimal region responsible for the potentiated phenotype observed in these N-terminal mutants. To this end, we performed smaller deletions and chimeras with other TRPM channels, including the chicken ortholog of TRPM8. Replacing the first 40 amino acids of TRPM8 with the corresponding residues of TRPM2 (1–57M2/M8) (see Fig. 1*E*) had the same effect as the 1–40 V1/M8 chimera, *i.e.* augmented responses to both agonists. This result suggests that the equivalent first residues of TRPM2 are not able to exert the same inhibitory effect as the initial 40 amino acids of TRPM8 (Fig. 5). Additionally, it has been reported that chicken TRPM8 (cTRPM8) exhibits enhanced sensitivity to cold and menthol (35). Also, compared with mTRPM8, it lacks the first nine amino acids (35). Thus, we tested a chimera encompassing the initial cTRPM8 sequence (1–30cM8/mM8). However, this construct displayed the same responses to agonists as the mM8-myc channel, suggesting that the putative inhibitory region is conserved in these two species and is not located within the region of the first nine amino acids (Fig. 5).

In a different set of experiments, using the mTRPM8-YFP sequence as a template, we performed two smaller deletions within the N terminus (Δ12–24 mTRPM8-YFP and Δ30–39 mTRPM8-YFP). Both deletions displayed the same increased responses to cold and menthol as the Δ5–39 mM8-YFP con-

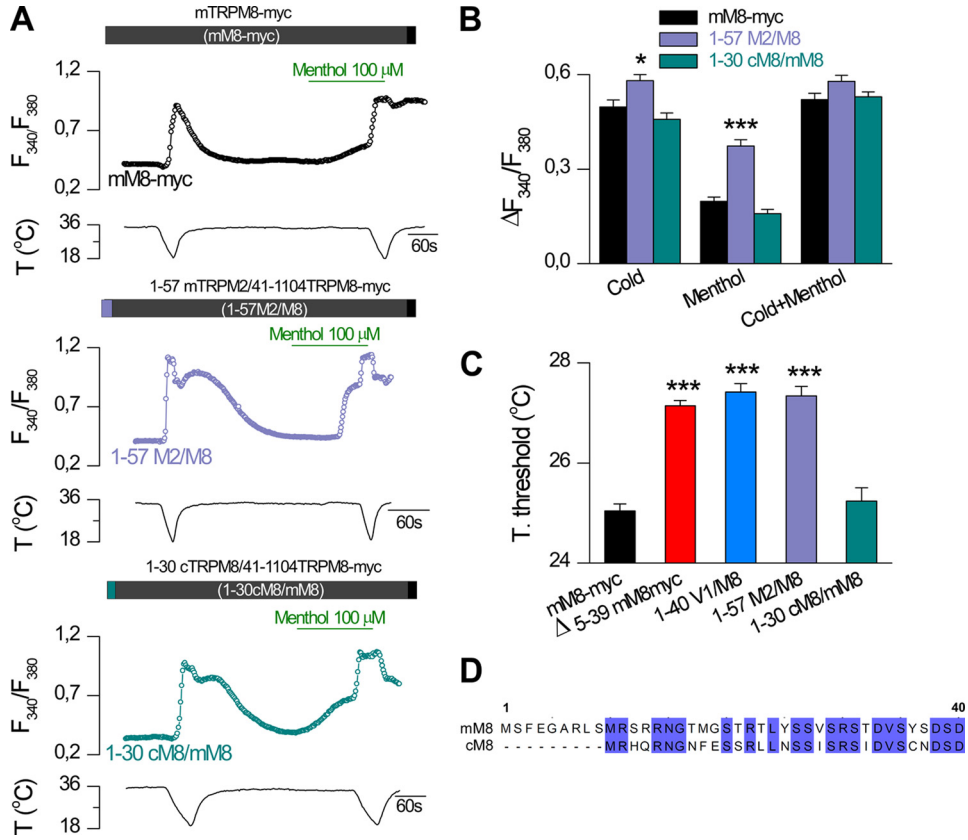

FIGURE 5. **Equivalent residues of TRPM2 do not induce the same inhibitory effect as the initial 40 amino acids of TRPM8.** *A,* representative intracellular calcium imaging traces showing responses to cold and 100 μM menthol in cells expressing TRPM8-myc (*mM8-myc*, *black, upper panel*), 1–57 mTRPM2/41–1104mTRPM8-myc (*1–57M2/M8*, *purple, middle panel*) and 1–30 cTRPM8/41–1104mTRPM8 (*1–30 cM8/mM8*, *green, bottom panel*). *B,* summary histogram of the mean ± S.E. calcium elevations obtained for the experimental protocol in *A*. Statistical significance was assessed with a one-way ANOVA test in combination with a Dunnett's post hoc test: *, $p < 0.05$; ***, $p < 0.001$ to mM8-myc, $n = 84$; 1–57 M2/M8, $n = 80$; 1–30 cM8/mM8, $n = 104$. *C,* mean ± S.E. temperature thresholds exhibited by transfected HEK293 cells with different constructs. Temperature thresholds were compared using a one-way ANOVA test in combination with Dunnett's post hoc correction: ***, $p < 0.001$ to mM8-myc (*mM8-myc*, $n = 564$; Δ5–39, $n = 334$; *1–40 V1/M8*, $n = 234$; *1–57 M2/M8*, $n = 80$; *1–30 cM8/mM8*, $n = 104$). *D,* alignment of the amino acid sequences of mouse and chicken TRPM8 using Clustal Omega and Jalview. *Numbers* correspond to residues in mTRPM8.

struct, suggesting that structural changes of the 12–39 region can lead to the enhanced activity exhibited by these mutants (Fig. 6). This finding was followed by the design of an additional set of smaller chimeras, using the HA epitope to replace short stretches of the mTRPM8-myc original sequence. In the functional analysis of these chimeras, we compared responses to cold and menthol, the temperature threshold of activation, and the expression levels of all the mutants used in these experiments. The results for all the different chimeras were normalized to control values (mM8-myc) and are shown in Fig. 7. To consider a mutant functionally equivalent to the hypersensitive initial deletion (Δ5–39), it had to fulfill three criteria as follows: an increase in the response amplitude to cold, a decrease in the temperature threshold, and an augmented response to 100 μM menthol at 34 °C. In this way, the region encompassing amino acids 20–30 was identified as responsible for the hypersensitive phenotype (Fig. 7, *A–C*). Interestingly, an opposite phenotype was observed in the 10–20HA mutant. A similar result was found in S9A and T17A mutants, which exhibited a decreased response to icilin (54). A second round of mutations reduced the critical inhibitory stretch to amino acids 25–28. Finally, the double mutant S26V/S27P was sufficient to fully recapitulate the behavior of the Δ5–39 mutant (Fig. 7, *A–C*). Positions Ser-26 and Ser-27 are putative sites for polyester poly-(*R*)-3-hydroxybutyrate modification (55) and PKC phosphorylation, according to phosphorylation prediction software (56). Considering that both modifications could participate in the modulation of channel activity (55, 57), we could not exclude that the observed effect was due to removal of these putative post-translational modifications sites. To address this question, we performed single point mutants where positions 26 and 27 were substituted by three different amino acids as follows: an amino acid lacking a hydroxyl group (S26V and S27A), amino acids that mimicked the phosphorylation (S26D and S27D), and finally, a substitution by proline (S26P and S27P), a residue that can act as a structural disruptor in the middle of regular secondary structure elements (58). Importantly, the only mutations that displayed increased responses to cold and menthol, along with a shift in the temperature threshold, were proline substitutions at positions 26 and 27 (Fig. 7, *A–C*). To examine whether functional changes produced by these mutations could be explained by systematic effects on channel expression, we analyzed expression levels by Western blot. As shown in Fig. 7*D*, protein levels for all the mutant constructs were similar to the control values, ruling out this possibility.

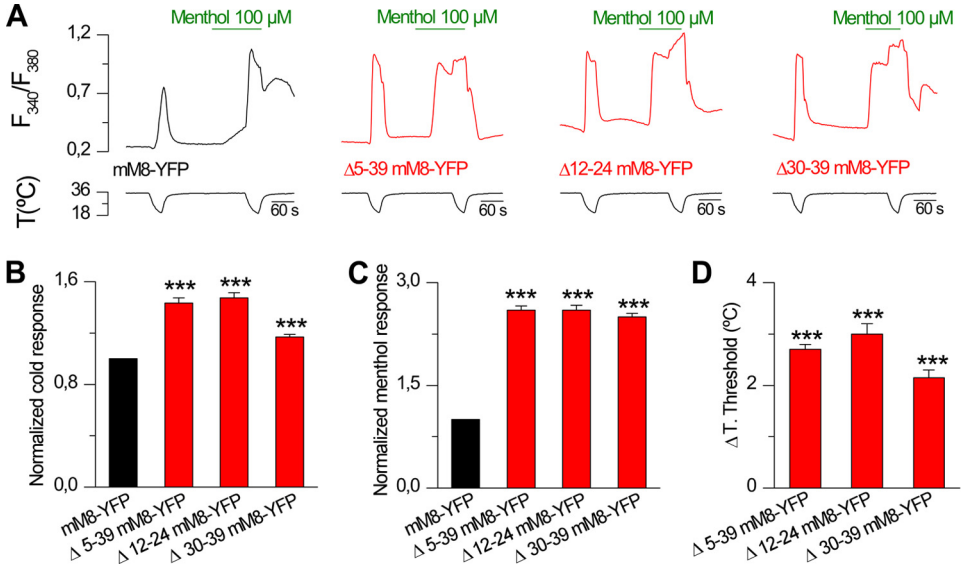

FIGURE 6. **Nonoverlapping deletions Δ12–24 and Δ30–39 display an enhanced activity to cold and menthol.** *A,* representative intracellular calcium imaging traces showing responses to cold and 100 μM menthol in cells expressing mTRPM8-YFP (*mM8-YFP*), Δ5–39 mTRPM8-YFP (*Δ5–39 mM8-YFP*), Δ12–24 TRPM8-YFP (*Δ12–24-mM8-YFP*), and Δ30–39 mTRPM8-YFP (*Δ30–39 mM8-YFP*). *B–D,* summary histogram of the mean ± S.E. amplitude of calcium responses to cold, menthol, and mean shift in temperature thresholds. The values were normalized to the mean response observed on mM8-YFP (control condition) (Δ5–39 mM8-YFP, $n = 100$; Δ12–24 mM8-YFP, $n = 66$; Δ30–39 mM8-YFP, $n = 137$). Statistical significance was assessed by an ANOVA test in combination with a Dunnett's post hoc test: ***, $p < 0.001$.

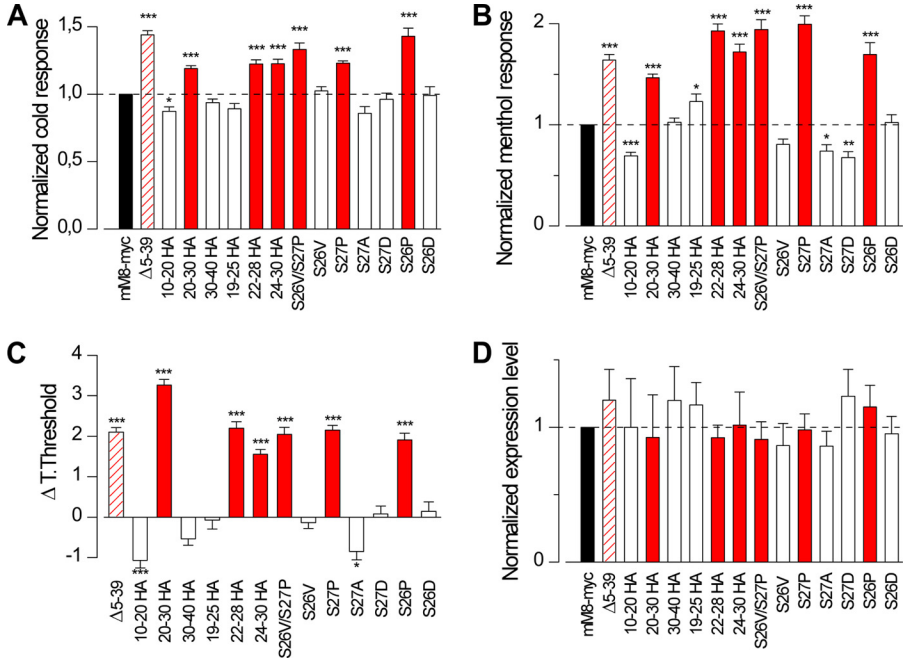

FIGURE 7. **Distal N-terminal region affects channel sensitivity to agonists.** Summary histogram of the responses to cold (*A*) and menthol (*B*) of the 13 TRPM8 mutants characterized in this part of the study. The values were normalized to the mean response observed on mM8-myc (control condition) in parallel experiments. *Black column* represents the mM8-myc value; *white columns* correspond to mutants that displayed a behavior similar to mM8-myc (control); and *red columns* represent mutants with an enhanced phenotype similar to Δ5–39 (10–20 HA, $n = 166$; 20–30HA, $n = 249$; 30–40 HA, $n = 277$; 19–25 HA, $n = 95$; 22–28 HA, $n = 132$; 24–30 HA, $n = 122$; SS2627VP, $n = 84$; S26V, $n = 180$; S27P, $n = 166$; S27A, $n = 88$; S2D, $n = 109$; S26P, $n = 166$; S26D, $n = 90$). Values in Δ5–39 (*striped red*) from Fig. 4 are displayed as reference. *C, bar histogram* of mean shift in temperature threshold displayed by each mutant referred to mM8-myc values. Positive values indicate shifts to warmer temperatures (same *n* as in *A* and *B*). *A–C,* statistical significance was assessed by an ANOVA test in combination with a Dunnett's post hoc test: *, $p < 0.05$; **, $p < 0.01$; ***, $p < 0.001$. *D,* quantification of Western blot experiments. Band intensities from at least three independent experiments were quantified and normalized to GAPDH expression as protein loading control. Levels were quantified relative to mM8-myc expression set at 1.0 ($n > 3$ for all the constructs).

S27P Mutation Facilitates the Gating of TRPM8 by Agonists—We decided to characterize further the agonist sensitivity of one of the hypersensitive single point mutants, the S27P channel, using the calcium imaging protocol shown in Fig. 8*A*. These experiments showed that, along with the observed shift in the cold temperature threshold toward higher temperatures (Fig. 8*B*), the S27P mutant is also more sensitive to menthol (Fig. 8, *A* and *C*). The EC_{50} value calculated from the S27P dose-response curves showed a 50% reduction compared with the mM8-myc value, probed in parallel experiments. Altogether, these results

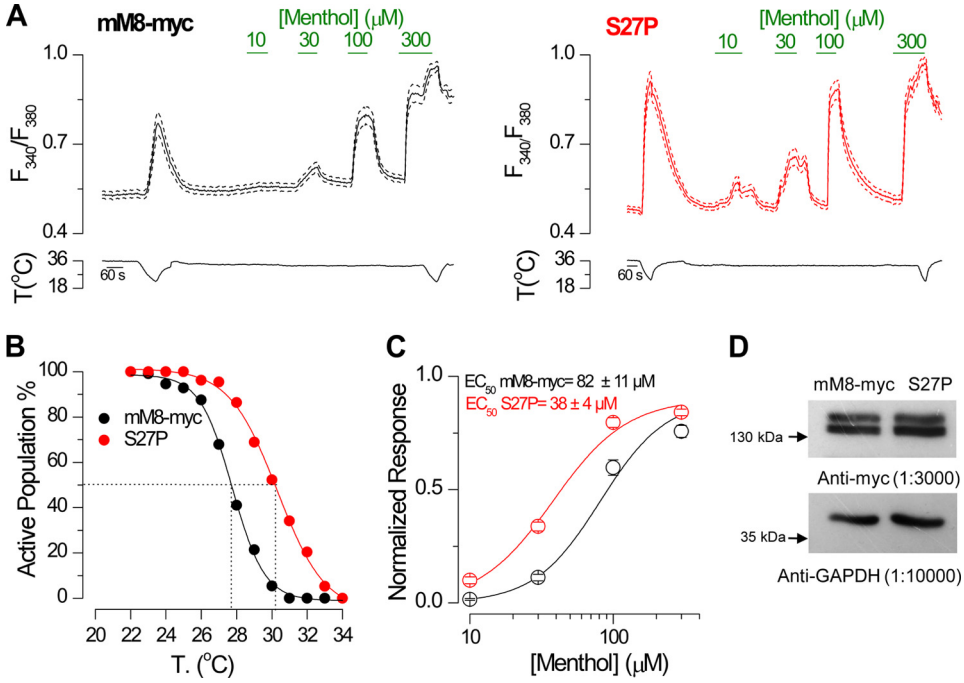

FIGURE 8. **S27P mutation is sufficient to mimic the Δ5–39 phenotype.** *A,* average (*solid line*) ± S.E. (*dotted lines*) time course of intracellular calcium level (F_{340}/F_{380}) in HEK293 cells (n >15 cells) transfected with mM8-myc (*black*) and S27P (*red*) channels during cooling ramps and applications of menthol at different concentrations. *B,* percentage of active population recruited during a cooling ramp in transfected HEK293 cells (mM8-myc, n = 112; S27P, n = 132). *C,* dose-response curves of intracellular calcium responses to menthol in transfected HEK293 cells. The *solid lines* represent a fit to the Hill equation that yielded an EC_{50} of 82 ± 11 μM for mM8-myc (n = 49) and 38 ± 4 μM for S27P (n = 80). Responses were normalized to the amplitude obtained with maximal stimulation (300 μM menthol plus cold). Recordings from wild type and mutant channels were interlaced on the same day. *D,* Western blots of lysates from HEK293 cells transfected with mM8-myc and S27P, probed with an anti-Myc antibody and anti-GAPDH as a loading control.

indicate that the S27P mutation is sufficient to obtain channels with increased sensitivity to both agonists, cold and menthol.

To explore the molecular mechanism that might explain the enhanced sensitivity to agonists displayed by the S27P mutant, we examined its electrophysiological properties using whole-cell patch clamp recordings in transfected HEK293 cells. We found that cells expressing the S27P mutant channel displayed a marked increase in response amplitude to agonists at −60 mV (I_{cold} = −5.9 ± 2.2 pA/pF; $I_{menthol}$ = −3.7 ± 1.1 pA/pF; $I_{cold+menthol}$ = −55.1 ± 8.9 pA/pF) compared with cells transfected with the mM8-myc channel (I_{cold} = −0.5 ± 0.2 pA/pF; $I_{menthol}$ = −0.7 ± 0.5 pA/pF; and $I_{cold+menthol}$ = −19.3 ± 5.7 pA/pF) (Fig. 9*C*). In lieu of the voltage dependence of TRPM8 channel gating (13, 18), we decided to compare the biophysical parameters associated with this potentiation. We hypothesized that the mechanism underlying the higher temperature threshold and menthol sensitivity displayed by the S27P mutant could be due to a shift in the voltage dependence of channel activation toward more negative membrane potentials. As predicted, the S27P mutant showed a large shift in the $V_{½}$ of activation of nearly −50 mV compared with the mM8-myc channel (Fig. 9*D*), with no change in maximal conductance (Fig. 9*E*) or slope factor (36 ± 5 mV^{-1}, mM8-myc *versus* 40 ± 4 mV^{-1}, S27P, cold; 40 ± 3 mV^{-1}, mM8-myc *versus* 41 ± 3 mV^{-1}, S27P, menthol; 48 ± 2 mV^{-1}, mM8-myc *versus* 50.2 ± 4.3 mV^{-1}, S27P, cold plus menthol). These results indicate that the increased sensitivity to agonist displayed by the S27P mutant is due primarily to a shift in the voltage activation curve toward physiologically relevant membrane potentials.

In summary, here we identified two nearby regions within the distal part of the N-terminal domain of TRPM8 that play a critical role in channel function. Region 40–60 plays a primary role in channel biogenesis, whereas the region encompassing the first 40 amino acids are critical for tuning the thermal and chemical sensitivity of this polymodal ion channel.

DISCUSSION

Very little is known about the role of the N terminus in the proper folding, assembly, and trafficking of TRPM8. Here, we studied in detail the first 60 amino acids of TRPM8 and were able to identify two separate regions with key roles in channel biogenesis and function. In other TRP channels, including some TRPMs, it has been reported that mutations or removal of the N-terminal region abrogate their function (27, 43, 51, 59–61). However, the underlying molecular mechanisms remain poorly understood. For example, TRPM2 channels with a deletion of the sequence upstream of the first MHR region are virtually absent from the cell surface (60), suggesting that this region is required for normal multimeric channel assembly and/or normal surface trafficking (60). Also, a truncation of the first 177 amino acids in the N terminus of TRPM4 renders nonfunctional channels that have a dominant negative effect on wild type TRPM4 currents (59), emphasizing the important role of the N terminus, and specifically its first amino acids, in proper channel assembly and function. Concerning previous studies focusing on the N terminus of TRPM8, Erler *et al.* (26), using a bacterial two-hybrid assay to analyze protein interactions, suggested the possible role of a weaker coiled-coil region

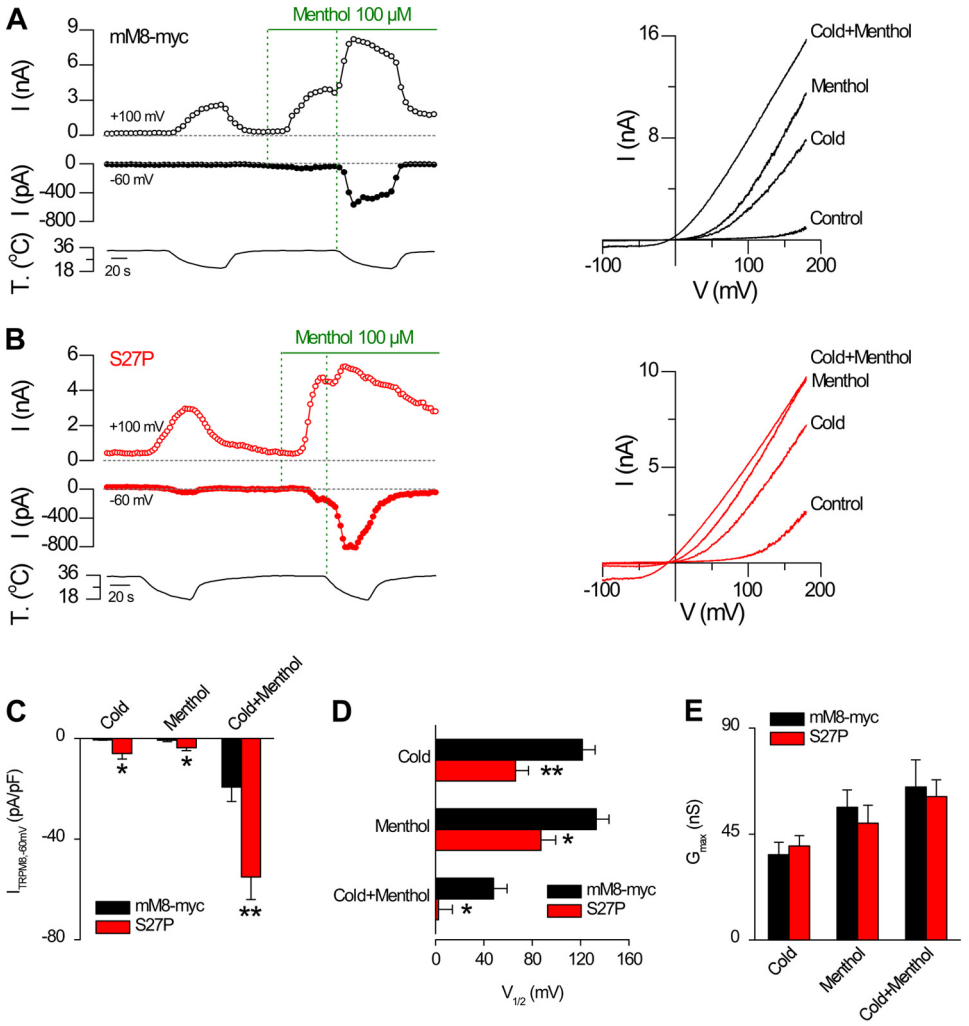

FIGURE 9. **S27P mutant shows facilitation of channel gating by agonists.** *A,* representative recording of whole-cell currents measured at +100 and −60 mV in HEK293 cell transfected with mM8-myc channels. Whole-cell capacitance of this cell is 13 pF. *Traces* on the *right* are current-voltage relationships of mM8-myc-transfected cells at 34 °C in control solution (*control*), at 20 °C in control solution (*cold*), at 34 °C in control solution supplemented with 100 μM menthol (*menthol*), and at 20 °C during a stimulus of 100 μM menthol (*cold plus menthol*). *B,* same experimental protocol as in *A* but on a representative cell transfected with the S27P channel. Whole-cell capacitance for the cell in *B* is 15 pF. *C, bar graph* summary of the mean ± S.E. values of maximal current density at −60 mV under the different conditions tested *(cold, menthol*, and *cold plus menthol*) obtained in experiments like *A* and *B*. *D* and *E*, mean values of $V_{1/2}$ and G_{max} obtained from the fits of the currents to Equation 1; *black bars* correspond to mM8-myc and *red bars* to S27P channels. Recordings from mM8-myc and mutant channels were always interlaced on the same day. Statistical significance was assessed with a two-tailed unpaired Student's *t* test: *, $p < 0.05$; **, $p < 0.01$, $n > 6$ cells for each condition.

within the proximal N-terminal region (residues 594–628) in the oligomerization of TRPM8 subunits. In addition, an *in silico* model of the quaternary structure suggests that the N terminus could be implicated in stabilization of the tetramer (37).

Role of the 40–60-Residue Region in Channel Biogenesis—A previous study showed that the 40–86-residue region of the TRPM8 N terminus is involved in channel trafficking to the plasma membrane and was the first to point out that the initial N terminus is important for channel function (27). One of the objectives of the this study was to characterize these alterations mechanistically. In the following paragraphs, we will argue that the functional deficits reside in proper folding and assembly.

The reduced expression on the cell surface of the deletion mutants of the N terminus of TRPM8 reported by Phelps and Gaudet (27) may be the end result of different processes. One process involves alteration in the normal trafficking of the proteins, *i.e.* the deletion affects the interaction between the protein and the trafficking machinery, resulting in accumulation within the ER. Alternatively, the deletion could unmask a retention/retrieval sequence, with equivalent results, net accumulation of the ion channel in the ER (62). The requirement of cytosolic domains for correct subcellular trafficking has been described for other TRP channels. For example, the interaction of the N terminus of TRPV4 with the PACSIN3 protein increases the plasma membrane levels of TRPV4 (63). Also, different sequence motifs contained in the N- and C-terminal regions are necessary for the dynamic localization of the *Drosophila* transient receptor potential-like channel between the rhabdomere and storage compartment in the cell body of photoreceptor cells (64). These two studies are examples of the regulation mechanisms involved in the proper targeting of functional ion channels to the plasma membrane. However, even before the correct targeting occurs, proper folding and assembly need to take place for subsequent transport to the

plasma membrane. Numerous studies indicate that ER export is limited primarily by quality control (47). For example, studies of several splice variants or TRP channel mutants reported their accumulation in the endoplasmic reticulum due to misfolding or compromised tetramerization rather than trafficking regulation mechanisms (22, 43, 51). In addition, it is possible that truncations that affect the quaternary structure also impair channel assembly and function. Thus, evaluating channel function represents a key step to distinguish between these two scenarios. To determine whether the TRPM8 N terminus is involved in its trafficking modulation to the plasma membrane or its proper folding and/or assembly, it is important to evaluate the activity of TRPM8 not only in the plasma membrane but also in the ER compartment.

Wild type TRPM8 can form functional ion channels in the ER compartment, whose activation can be monitored using calcium imaging techniques (32, 48–50). Moreover, we showed previously that the combined stimulation with cold and menthol (32) circumvents the use of high concentrations of menthol that could release calcium from intracellular compartments through a TRPM8-independent mechanism (65). In HEK293 cells transfected with wild type TRPM8, the calcium responses to cold plus menthol have two components. The main component corresponds to the activity of TRPM8 channels located in the plasma membrane, although a minor fraction of the response (~15%) arises from channels in the ER compartment. This small contribution to the net response could be the result of a lower presence of TRPM8 in the ER compartment, problems with menthol accessibility to inner membranes, and/or changes in the activation properties of the channel in this location. In agreement with our results, TRPV1 channels located in the ER also need a saturating concentration of capsaicin to elicit a detectable response (66). However, despite the lower activity of TRPM8 within this compartment, if the deletions render properly folded and assembled channels, and the retention in the ER compartment is due to changes in trafficking modulation, it should be possible to observe a response when cold and menthol are applied together. In contrast to this expectation/hypothesis, we established that deletion of a region encompassing positions 40–60 of the N-terminal domain (Δ41–57) fully abolishes TRPM8 activity. This mutant is mainly localized within the ER, explaining their lack of mature glycosylation. Co-immunoprecipitation experiments showed that the Δ41-57 deletion does not prevent its biochemical interaction with wild type TRPM8 subunits. However, the results of FRET suggest that this deletion caused major alterations in the interaction between subunits. These changes in quaternary structure could explain both the lack of activity and the ER retention, considering that minor deviations from native conformation can elicit such phenomena (47). Moreover, retention in the ER can occur even if the tetramerization of the channel is not prevented. For example, the Δ1–38 TRPV5 mutant produces a nonfunctional channel that lacks mature glycosylation and is mainly located in the ER (51). In the study, the authors investigated the oligomerization state of the deletion using the perfluorooctanoic acid-PAGE technique and concluded that although formation of the tetramer occurs, the Δ1–38 subunits were probably not folded correctly and were therefore retained in the ER (51). This observation is an example of ER retention of a multimeric channel that is not the result of defects in tetramerization but is rather caused by the misfolding of the subunits. In fact, mutations of TRPM8 that appear to impact the formation of the tetramer (22, 26), as well as other mutations without defects in oligomerization (27), result in the same phenotype, characterized by lack of functionality, absence of mature *N*-glycosylation, and impaired trafficking to the plasma membrane (22, 26, 27, 67). In this study we have not assessed the oligomerization state of the deletion mutant, but it could be expected that, similarly to the N-terminal deletions reported previously in the work of Phelps and Gaudet (27), our deletions inside the 40–60-residue region would not prevent tetramerization.

Our next goal was to identify the key residues responsible for the nonfunctional phenotype. Using chimeras between TRPM2 and TRPM8, we observed ER retention when the 50–59-residue region of TRPM8 was substituted by the 66–76-residue stretch of TRPM2. This chimera (50–59M2/M8) also lacked mature *N*-glycosylation, in agreement with its main distribution in the ER compartment. Nevertheless, it did not exhibit a complete loss of activity, although the responses to cold and menthol were largely impaired. It is important to emphasize that both calcium imaging experiments in zero calcium and electrophysiological experiments clearly demonstrated that the responses of the 50–59M2/M8 chimera were mediated by channels expressed in the plasma membrane, a result that may seem contradictory with the main ER localization displayed by this mutant. Furthermore, the lack of complex glycosylation observed also suggests that these channels do not transit through the Golgi apparatus. Alternative routes to direct proteins to the plasma membrane bypassing the Golgi have been described (68). In fact, de Groot *et al.* (51) have shown that the nonfunctional Δ1–38 TRPV5 escaped the endoplasmic reticulum quality control, appearing at the plasma membrane without being processed by the Golgi apparatus. In a similar way, our experiments demonstrate that the 50–59M2/M8 chimera, despite an important reduction of the surface expression, can also reach the cell surface without displaying any apparent mature *N*-glycosylation, suggesting that these channels bypass the Golgi. Moreover, in agreement with our previous results where we reported that TRPM8 channels lacking *N*-glycosylation showed a shift in the voltage dependence curve toward more positive membrane potentials (32), this chimera exhibits the same alteration in the gating by agonists. However, it cannot be ruled out that the mutations within the N terminus may also cause the alterations observed in the biophysical properties of this construct.

In the 50–59M2/M8 chimera, only four amino acids differed from the wild type TRPM8 protein; of these, we found that T58V and R59E are involved in the functional defect that we observed. Interestingly, these amino acids are still present in the completely nonfunctional Δ41–57 construct. We assume that the large deletion probably changes their position in the quaternary structure, resulting in the impaired activity and ER retention observed.

In summary, the first part of our results agree with and refine a previous study that showed that the N-terminal region that precedes the first MHR alters plasma membrane localization of

TRPM8 (27). We show that the 40–60-residue region of the N terminus of TRPM8 is important to generate functional channels in the plasma membrane. Nevertheless, although our results suggest that the reduced level of channels on the cell surface is caused by alterations in folding and/or assembly that lead ER retention and lack of function, it is not possible to completely rule out defects in other trafficking mechanisms that could also contribute to this phenomenon.

These findings may have pathophysiological relevance, because an isoform of hTRPM8b expressed in cancer cell lines displays an alternative N-terminal domain. TRPM8 and hTRPM8b have the same sequence from residue 65 onward (41, 49). Before this residue, TRPM8b contains an initial region that consists of 15 amino acids with a different sequence to those observed in the full-length isoform at the equivalent positions, *i.e.* 50–64. Therefore, this variant represents an endogenous deletion of the first 65 amino acids of TRPM8. As our results predicted, this isoform lacked mature glycosylation and displayed a distribution pattern that suggested ER accumulation. Moreover, in agreement with our deletion experiments in the region encompassing the 40–60 positions in murine constructs, this human splice isoform did not exhibit responses to any of the stimuli applied, suggesting that it is completely nonfunctional. Considering that our co-immunoprecipitation experiments showed that the Δ41-57 construct interacts with the wild type channel and that the hTRPM8b isoform and the hTRPM8 full-length protein are expressed simultaneously in some prostate cancer cell lines, at least at the mRNA level (49), hTRPM8b could function as a dominant negative, sequestering the hTRPM8 subunits and decreasing the formation of functional TRPM8 channels in the plasma membrane (41). Further studies are necessary to explore this possibility in native tissues.

Initial 40 Amino Acids Act as an Inhibitory Region in TRPM8 Activation by Cold and Menthol—We also showed that the first 40 amino acids of TRPM8 act as an inhibitory region on channel activity. An increase in TRPM8 activity, similar to that produced by the truncation of this entire region, is achieved by nonoverlapping deletions as follows: Δ12–24 and Δ30–39 or the introduction of a single proline at positions 26 or 27, suggesting that these deletions and substitutions lead to equivalent structural changes that result in the same potentiated phenotype. A crystal structure of this region would certainly provide important insight regarding the spatial interactions between the different amino acids in this segment of the protein.

Electrophysiological analysis of the S27P mutant determined that the potentiation in the response to cold or menthol is due to a leftward shift of ~50 mV in the voltage dependence of activation, increasing the probability of channel opening at more physiological membrane potentials. The fact that this phenotype occurs only when a proline is introduced, without a significant effect of alanine or aspartate mutations, indicates that these two serines *per se*, or putative post-translational modifications in these residues, are not playing a critical role in this inhibition. In contrast, our results suggest that the introduction of a proline at position 27 alters the structure of TRPM8. Proline has a rigid pyrrolidine ring as a side chain, and its substitution in the middle of an α-helix or a β-sheet can disrupt the secondary structure of the protein (58). For example, it has been suggested that the mutation of leucine 1089 to a proline in TRPM8 induces a break in the heptahelical repeat region disrupting the coiled-coil structure, thereby affecting the proper tetramerization of the channel (26). We ran different programs to predict the secondary structure of TRPM8 (69–71), but they did not show consensus in the putative secondary structure of the first 40 amino acids. However, different algorithms used to identify disordered regions assign a high score to this region (72). It is well known that many proteins have regions with very flexible and unstable structures, even in their native states. Such proteins or regions are referred to as being natively disordered or unstructured (73). The flexibility of disordered polypeptides allows the same amino acid sequence to adopt multiple conformations and thereby interact with different ligands (74). In the case of ion channels, it has been reported that disorder often occurs in their cytoplasmic domains (75, 76) and that in some cases this phenomenon determines their activation properties. For example, by altering the conformation of the disordered cytoplasmic domains, it is possible to uncouple physiological regulation of the NMDA receptor by extracellular Zn^{2+} (77).

We speculate that, in wild type TRPM8 channels, the interaction of the N-terminal region with other TRPM8 domains or with a partner protein reduce channel activity. Interestingly, the $G\alpha_q$ protein interacts directly with both the N- and C-terminal domains of TRPM8, resulting in direct channel inhibition following activation of G-protein-coupled receptors (78). Moreover, in that study, the authors showed that binding of endogenous $G\alpha_q$ imposes a tonic inhibition on TRPM8 (78). One possible explanation for the observed increased activity after deletion of the first 40 amino acids of TRPM8 is the absence of an interaction with $G\alpha_q$, or other modulatory proteins, that constitutively inhibits TRPM8 function. We cannot exclude the possibility that the potentiation observed is due to the loss of interactions of this domain with other sequences in the TRPM8 homotetramer, preventing its role as an internal inhibitor region. Because the quaternary structure determines the precise biophysical properties displayed by an ion channel, it is also possible that deletion of the first 40 amino acids produces structural changes that lead to a gain-of-function phenotype. Interestingly, residues Ser-9 and Thr-17 have been postulated to act as PKA targets with subsequent effects in TRPM8 activity (54). Using site-directed mutagenesis, the authors demonstrated that mutants S9A and T17A displayed reduced responses to icilin compared with the wild type channel, and they concluded that phosphorylation alters the activity of TRPM8 (54). Together with these results, our observations reinforce the idea that the initial N-terminal region is important in tuning the response of TRPM8 to its canonical agonists; mutations S9A and T17A can produce an increase in the inhibitory effect of this region, whereas the deletions inside this region or S26P and S27P mutations are able to remove it.

In conclusion, our report shows that two distinct regions within the first 60 amino acids of TRPM8 are involved in different aspects of its biogenesis and function. The region encompassing positions 40–60 is critical for the genesis of a functional channel. Deletion of this region, and in particular mutation of residues Thr-58 and Arg-59, results in impaired

channel activity and ER retention. In contrast, deletion of the first 40 amino acids results in a gain-of-function phenotype, explained by changes in channel gating. Single point mutations of Ser-27 and Ser-26 to proline mimic the effect of truncation of the initial part of the N-terminal region of the channel, suggesting that a structural break on this region is sufficient to modify the constitutive inhibitory role of this small domain in the function of TRPM8.

Acknowledgments—We thank Dr. Annika Mälkiä for comments to the manuscript, and Jeremy Salas, Bastián Rivera, Ana Miralles, and the late Alfonso Pérez-Vegara for excellent technical assistance.

REFERENCES

1. Hensel, H., and Zotterman, Y. (1951) The response of the cold receptors to constant cooling. *Acta Physiol. Scand.* **22,** 96–105
2. Heppelmann, B., Messlinger, K., Neiss, W. F., and Schmidt, R. F. (1990) Ultrastructural three-dimensional reconstruction of group III and group IV sensory nerve endings ("free nerve endings") in the knee joint capsule of the cat: evidence for multiple receptive sites. *J. Comp. Neurol.* **292,** 103–116
3. Iriuchijima, J., and Zotterman, Y. (1960) The specificity of afferent cutaneous C fibre. *Acta Physiol. Scand.* **49,** 267–278
4. Pertusa, M., Moldenhauer, H., Brauchi, S., Latorre, R., Madrid, R., and Orio, P. (2012) in *Mutagenesis* (Rajnikant Mishra, ed) pp. 221–246, In-Tech, Rijeka, Croatia
5. Talavera, K., Nilius, B., and Voets, T. (2008) Neuronal TRP channels: thermometers, pathfinders and life-savers. *Trends Neurosci.* **31,** 287–295
6. Vay, L., Gu, C., and McNaughton, P. A. (2012) The thermo-TRP ion channel family: properties and therapeutic implications. *Br. J. Pharmacol.* **165,** 787–801
7. Almaraz, L., Manenschijn, J. A., de la Peña, E., and Viana, F. (2014) Trpm8. *Handb. Exp. Pharmacol.* **222,** 547–579
8. Latorre, R., Brauchi, S., Madrid, R., and Orio, P. (2011) A cool channel in cold transduction. *Physiology* **26,** 273–285
9. Madrid, R., and Pertusa, M. (2014) Intimacies and physiological role of the polymodal cold-sensitive ion channel TRPM8. *Curr. Top. Membr.* **74,** 230–260
10. McCoy, D. D., Knowlton, W. M., and McKemy, D. D. (2011) Scraping through the ice: uncovering the role of TRPM8 in cold transduction. *Am. J. Physiol. Regul. Integr. Comp. Physiol.* **300,** R1278–R1287
11. McKemy, D. D., Neuhausser, W. M., and Julius, D. (2002) Identification of a cold receptor reveals a general role for TRP channels in thermosensation. *Nature* **416,** 52–58
12. Peier, A. M., Moqrich, A., Hergarden, A. C., Reeve, A. J., Andersson, D. A., Story, G. M., Earley, T. J., Dragoni, I., McIntyre, P., Bevan, S., and Patapoutian, A. (2002) A TRP channel that senses cold stimuli and menthol. *Cell* **108,** 705–715
13. Brauchi, S., Orio, P., and Latorre, R. (2004) Clues to understanding cold sensation: thermodynamics and electrophysiological analysis of the cold receptor TRPM8. *Proc. Natl. Acad. Sci. U.S.A.* **101,** 15494–15499
14. Zakharian, E., Cao, C., and Rohacs, T. (2010) Gating of transient receptor potential melastatin 8 (TRPM8) channels activated by cold and chemical agonists in planar lipid bilayers. *J. Neurosci.* **30,** 12526–12534
15. de la Peña, E., Mälkiä, A., Cabedo, H., Belmonte, C., and Viana, F. (2005) The contribution of TRPM8 channels to cold sensing in mammalian neurones. *J. Physiol.* **567,** 415–426
16. Madrid, R., Donovan-Rodríguez, T., Meseguer, V., Acosta, M. C., Belmonte, C., and Viana, F. (2006) Contribution of TRPM8 channels to cold transduction in primary sensory neurons and peripheral nerve terminals. *J. Neurosci.* **26,** 12512–12525
17. Mälkiä, A., Madrid, R., Meseguer, V., de la Peña E., Valero, M., Belmonte, C., and Viana, F. (2007) Bidirectional shifts of TRPM8 channel gating by temperature and chemical agents modulate the cold sensitivity of mammalian thermoreceptors. *J. Physiol.* **581,** 155–174
18. Voets, T., Droogmans, G., Wissenbach, U., Janssens, A., Flockerzi, V., and Nilius, B. (2004) The principle of temperature-dependent gating in cold- and heat-sensitive TRP channels. *Nature* **430,** 748–754
19. Clapham, D. E. (2003) TRP channels as cellular sensors. *Nature* **426,** 517–524
20. Janssens, A., and Voets, T. (2011) Ligand stoichiometry of the cold- and menthol-activated channel TRPM8. *J. Physiol.* **589,** 4827–4835
21. Stewart, A. P., Egressy, K., Lim, A., and Edwardson, J. M. (2010) AFM imaging reveals the tetrameric structure of the TRPM8 channel. *Biochem. Biophys. Res. Commun.* **394,** 383–386
22. Tsuruda, P. R., Julius, D., and Minor, D. L., Jr. (2006) Coiled coils direct assembly of a cold-activated TRP channel. *Neuron* **51,** 201–212
23. Latorre, R., Brauchi, S., Orta, G., Zaelzer, C., and Vargas, G. (2007) ThermoTRP channels as modular proteins with allosteric gating. *Cell Calcium* **42,** 427–438
24. Montell, C. (2001) Physiology, phylogeny, and functions of the TRP superfamily of cation channels. *Sci. STKE 2001,* 10.1126/stke.2001.90.re1
25. Rohács, T., Lopes, C. M., Michailidis, I., and Logothetis, D. E. (2005) $PI(4,5)P_2$ regulates the activation and desensitization of TRPM8 channels through the TRP domain. *Nat. Neurosci.* **8,** 626–634
26. Erler, I., Al-Ansary, D. M., Wissenbach, U., Wagner, T. F., Flockerzi, V., and Niemeyer, B. A. (2006) Trafficking and assembly of the cold-sensitive TRPM8 channel. *J. Biol. Chem.* **281,** 38396–38404
27. Phelps, C. B., and Gaudet, R. (2007) The role of the N terminus and transmembrane domain of TRPM8 in channel localization and tetramerization. *J. Biol. Chem.* **282,** 36474–36480
28. Voets, T., Owsianik, G., Janssens, A., Talavera, K., and Nilius, B. (2007) TRPM8 voltage sensor mutants reveal a mechanism for integrating thermal and chemical stimuli. *Nat. Chem. Biol.* **3,** 174–182
29. Owsianik, G., Talavera, K., Voets, T., and Nilius, B. (2006) Permeation and selectivity of TRP channels. *Annu. Rev. Physiol.* **68,** 685–717
30. Dragoni, I., Guida, E., and McIntyre, P. (2006) The cold and menthol receptor TRPM8 contains a functionally important double cysteine motif. *J. Biol. Chem.* **281,** 37353–37360
31. Morenilla-Palao, C., Pertusa, M., Meseguer, V., Cabedo, H., and Viana, F. (2009) Lipid raft segregation modulates TRPM8 channel activity. *J. Biol. Chem.* **284,** 9215–9224
32. Pertusa, M., Madrid, R., Morenilla-Palao, C., Belmonte, C., and Viana, F. (2012) *N*-Glycosylation of TRPM8 ion channels modulates temperature sensitivity of cold thermoreceptor neurons. *J. Biol. Chem.* **287,** 18218–18229
33. Bandell, M., Dubin, A. E., Petrus, M. J., Orth, A., Mathur, J., Hwang, S. W., and Patapoutian, A. (2006) High-throughput random mutagenesis screen reveals TRPM8 residues specifically required for activation by menthol. *Nat. Neurosci.* **9,** 493–500
34. Malkia, A., Pertusa, M., Fernández-Ballester, G., Ferrer-Montiel, A., and Viana, F. (2009) Differential role of the menthol-binding residue Y745 in the antagonism of thermally gated TRPM8 channels. *Mol. Pain* **5,** 62
35. Chuang, H. H., Neuhausser, W. M., and Julius, D. (2004) The super-cooling agent icilin reveals a mechanism of coincidence detection by a temperature-sensitive TRP channel. *Neuron* **43,** 859–869
36. Fleig, A., and Penner, R. (2004) The TRPM ion channel subfamily: molecular, biophysical and functional features. *Trends Pharmacol. Sci.* **25,** 633–639
37. Pedretti, A., Marconi, C., Bettinelli, I., and Vistoli, G. (2009) Comparative modeling of the quaternary structure for the human TRPM8 channel and analysis of its binding features. *Biochim. Biophys. Acta* **1788,** 973–982
38. Vázquez, E., and Valverde, M. A. (2006) A review of TRP channels splicing. *Semin. Cell Dev. Biol.* **17,** 607–617
39. Sabnis, A. S., Shadid, M., Yost, G. S., and Reilly, C. A. (2008) Human lung epithelial cells express a functional cold-sensing TRPM8 variant. *Am. J. Respir. Cell Mol. Biol.* **39,** 466–474
40. Bidaux, G., Beck, B., Zholos, A., Gordienko, D., Lemonnier, L., Flourakis, M., Roudbaraki, M., Borowiec, A. S., Fernández, J., Delcourt, P., Lepage, G., Shuba, Y., Skryma, R., and Prevarskaya, N. (2012) Regulation of activity of transient receptor potential melastatin 8 (TRPM8) channel by its short isoforms. *J. Biol. Chem.* **287,** 2948–2962
41. Lis, A., Wissenbach, U., and Philipp, S. E. (2005) Transcriptional regula-

tion and processing increase the functional variability of TRPM channels. *Naunyn Schmiedebergs Arch. Pharmacol.* **371,** 315–324
42. Schneider, C. A., Rasband, W. S., and Eliceiri, K. W. (2012) NIH Image to ImageJ: 25 years of image analysis. *Nat. Methods* **9,** 671–675
43. Arniges, M., Fernández-Fernández, J. M., Albrecht, N., Schaefer, M., and Valverde, M. A. (2006) Human TRPV4 channel splice variants revealed a key role of ankyrin domains in multimerization and trafficking. *J. Biol. Chem.* **281,** 1580–1586
44. Hellwig, N., Albrecht, N., Harteneck, C., Schultz, G., and Schaefer, M. (2005) Homo- and heteromeric assembly of TRPV channel subunits. *J. Cell Sci.* **118,** 917–928
45. Nilius, B., Mahieu, F., Prenen, J., Janssens, A., Owsianik, G., Vennekens, R., and Voets, T. (2006) The Ca^{2+}-activated cation channel TRPM4 is regulated by phosphatidylinositol 4,5-biphosphate. *EMBO J.* **25,** 467–478
46. Ma, D., Zerangue, N., Lin, Y. F., Collins, A., Yu, M., Jan, Y. N., and Jan, L. Y. (2001) Role of ER export signals in controlling surface potassium channel numbers. *Science* **291,** 316–319
47. Ellgaard, L., and Helenius, A. (2003) Quality control in the endoplasmic reticulum. *Nat. Rev. Mol. Cell Biol.* **4,** 181–191
48. Thebault, S., Lemonnier, L., Bidaux, G., Flourakis, M., Bavencoffe, A., Gordienko, D., Roudbaraki, M., Delcourt, P., Panchin, Y., Shuba, Y., Skryma, R., and Prevarskaya, N. (2005) Novel role of cold/menthol-sensitive transient receptor potential melastatine family member 8 (TRPM8) in the activation of store-operated channels in LNCaP human prostate cancer epithelial cells. *J. Biol. Chem.* **280,** 39423–39435
49. Valero, M., Morenilla-Palao, C., Belmonte, C., and Viana, F. (2011) Pharmacological and functional properties of TRPM8 channels in prostate tumor cells. *Pflugers Arch.* **461,** 99–114
50. Zhang, L., and Barritt, G. J. (2004) Evidence that TRPM8 is an androgen-dependent Ca^{2+} channel required for the survival of prostate cancer cells. *Cancer Res.* **64,** 8365–8373
51. de Groot, T., van der Hagen, E. A., Verkaart, S., te Boekhorst, V. A., Bindels, R. J., and Hoenderop, J. G. (2011) Role of the transient receptor potential vanilloid 5 (TRPV5) protein N terminus in channel activity, tetramerization, and trafficking. *J. Biol. Chem.* **286,** 32132–32139
52. García-Sanz, N., Valente, P., Gomis, A., Fernández-Carvajal, A., Fernández-Ballester, G., Viana, F., Belmonte, C., and Ferrer-Montiel, A. (2007) A role of the transient receptor potential domain of vanilloid receptor I in channel gating. *J. Neurosci.* **27,** 11641–11650
53. Caterina, M. J., Schumacher, M. A., Tominaga, M., Rosen, T. A., Levine, J. D., and Julius, D. (1997) The capsaicin receptor: a heat-activated ion channel in the pain pathway. *Nature* **389,** 816–824
54. Bavencoffe, A., Gkika, D., Kondratskyi, A., Beck, B., Borowiec, A. S., Bidaux, G., Busserolles, J., Eschalier, A., Shuba, Y., Skryma, R., and Prevarskaya, N. (2010) The transient receptor potential channel TRPM8 is inhibited via the α2A adrenoreceptor signaling pathway. *J. Biol. Chem.* **285,** 9410–9419
55. Cao, C., Yudin, Y., Bikard, Y., Chen, W., Liu, T., Li, H., Jendrossek, D., Cohen, A., Pavlov, E., Rohacs, T., and Zakharian, E. (2013) Polyester modification of the mammalian TRPM8 channel protein: implications for structure and function. *Cell Rep.* **4,** 302–315
56. Blom, N., Sicheritz-Pontén, T., Gupta, R., Gammeltoft, S., and Brunak, S. (2004) Prediction of post-translational glycosylation and phosphorylation of proteins from the amino acid sequence. *Proteomics* **4,** 1633–1649
57. Premkumar, L. S., Raisinghani, M., Pingle, S. C., Long, C., and Pimentel, F. (2005) Downregulation of transient receptor potential melastatin 8 by protein kinase C-mediated dephosphorylation. *J. Neurosci.* **25,** 11322–11329
58. Pakula, A. A., and Sauer, R. T. (1989) Genetic analysis of protein stability and function. *Annu. Rev. Genet.* **23,** 289–310
59. Launay, P., Cheng, H., Srivatsan, S., Penner, R., Fleig, A., and Kinet, J. P. (2004) TRPM4 regulates calcium oscillations after T cell activation. *Science* **306,** 1374–1377
60. Perraud, A. L., Schmitz, C., and Scharenberg, A. M. (2003) TRPM2 Ca^{2+} permeable cation channels: from gene to biological function. *Cell Calcium* **33,** 519–531
61. Erler, I., Hirnet, D., Wissenbach, U., Flockerzi, V., and Niemeyer, B. A. (2004) Ca^{2+}-selective transient receptor potential V channel architecture and function require a specific ankyrin repeat. *J. Biol. Chem.* **279,** 34456–34463
62. Michelsen, K., Yuan, H., and Schwappach, B. (2005) Hide and run. Arginine-based endoplasmic-reticulum-sorting motifs in the assembly of heteromultimeric membrane proteins. *EMBO Rep.* **6,** 717–722
63. Cuajungco, M. P., Grimm, C., Oshima, K., D'hoedt, D., Nilius, B., Mensenkamp, A. R., Bindels, R. J., Plomann, M., and Heller, S. (2006) PACSINs bind to the TRPV4 cation channel. PACSIN 3 modulates the subcellular localization of TRPV4. *J. Biol. Chem.* **281,** 18753–18762
64. Richter, D., Katz, B., Oberacker, T., Tzarfaty, V., Belusic, G., Minke, B., and Huber, A. (2011) Translocation of the *Drosophila* transient receptor potential-like (TRPL) channel requires both the N- and C-terminal regions together with sustained Ca^{2+} entry. *J. Biol. Chem.* **286,** 34234–34243
65. Mahieu, F., Owsianik, G., Verbert, L., Janssens, A., De Smedt, H., Nilius, B., and Voets, T. (2007) TRPM8-independent menthol-induced Ca^{2+} release from endoplasmic reticulum and Golgi. *J. Biol. Chem.* **282,** 3325–3336
66. Gallego-Sandín, S., Rodríguez-García, A., Alonso, M. T., and García-Sancho, J. (2009) The endoplasmic reticulum of dorsal root ganglion neurons contains functional TRPV1 channels. *J. Biol. Chem.* **284,** 32591–32601
67. Kühn, F. J., Winking, M., Kühn, C., Hoffmann, D. C., and Lückhoff, A. (2013) Surface expression and channel function of TRPM8 are cooperatively controlled by transmembrane segments S3 and S4. *Pflugers Arch.* **465,** 1599–1610
68. Grieve, A. G., and Rabouille, C. (2011) Golgi bypass: skirting around the heart of classical secretion. *Cold Spring Harbor Perspect. Biol.* 10.1101/cshperspect.a005298
69. Chou, P. Y., and Fasman, G. D. (1974) Prediction of protein conformation. *Biochemistry* **13,** 222–245
70. Cole, C., Barber, J. D., and Barton, G. J. (2008) The Jpred 3 secondary structure prediction server. *Nucleic Acids Res.* **36,** W197–W201
71. Jones, D. T. (1999) Protein secondary structure prediction based on position-specific scoring matrices. *J. Mol. Biol.* **292,** 195–202
72. Linding, R., Jensen, L. J., Diella, F., Bork, P., Gibson, T. J., and Russell, R. B. (2003) Protein disorder prediction: implications for structural proteomics. *Structure* **11,** 1453–1459
73. Tompa, P. (2002) Intrinsically unstructured proteins. *Trends Biochem. Sci.* **27,** 527–533
74. Oldfield, C. J., Meng, J., Yang, J. Y., Yang, M. Q., Uversky, V. N., and Dunker, A. K. (2008) Flexible nets: disorder and induced fit in the associations of p53 and 14-3-3 with their partners. *BMC Genomics* **9,** S1
75. Minezaki, Y., Homma, K., and Nishikawa, K. (2007) Intrinsically disordered regions of human plasma membrane proteins preferentially occur in the cytoplasmic segment. *J. Mol. Biol.* **368,** 902–913
76. Xue, B., Li, L., Meroueh, S. O., Uversky, V. N., and Dunker, A. K. (2009) Analysis of structured and intrinsically disordered regions of transmembrane proteins. *Mol. Biosyst.* **5,** 1688–1702
77. Choi, U. B., Kazi, R., Stenzoski, N., Wollmuth, L. P., Uversky, V. N., and Bowen, M. E. (2013) Modulating the intrinsic disorder in the cytoplasmic domain alters the biological activity of the *N*-methyl-D-aspartate-sensitive glutamate receptor. *J. Biol. Chem.* **288,** 22506–22515
78. Zhang, X., Mak, S., Li, L., Parra, A., Denlinger, B., Belmonte, C., and McNaughton, P. A. (2012) Direct inhibition of the cold-activated TRPM8 ion channel by Gαq. *Nat. Cell Biol.* **14,** 851–858